Significance of geochemical signatures on provenance in intracratonic rift basins: Examples from the Iberian plate

M. Ochoa[†]
M.E. Arribas
J. Arribas
Departamento de Petrología y Geoquímica, Universidad Complutense de Madrid, 28040 Madrid, Spain

R. Mas
Departamento de Estratigrafía, Universidad Complutense de Madrid, 28040 Madrid, Spain

ABSTRACT

Following the Variscan orogeny, the Iberian plate was affected by an extensional tectonic regime from Late Permian to Late Cretaceous time. In the central part of the plate, NW-SE–trending rift basins were created. Two rifting cycles can be identified during the extensional stage: (1) a Late Permian to Hettangian cycle, and (2) a latest Jurassic to Early Cretaceous cycle. During these cycles, thick clastic continental sequences were deposited in grabens and half grabens. In both cycles, sandstone petrofacies from periods of high tectonic activity reveal a main plutoniclastic (quartzofeldspathic) character due to the erosion of coarse-grained crystalline rocks from the Hesperian Massif, during Buntsandstein (mean $Qm_{72}F_{25}Lt_3$) sedimentation and during Barremian–early Albian times (mean $Qm_{81}F_{18}Lt_1$). Geochemical data show that weathering was more intense during the second rifting phase (mean chemical index of alteration [CIA]: 80) due to more severe climate conditions (humid) than during the first rifting phase (mean CIA: 68) (arid climate).

Ratios between major and trace elements agree with a main provenance from passive-margins settings in terms of the felsic nature of the crust. However, anomalies in trace elements have been detected in some Lower Cretaceous samples, suggesting additional basic supplies from the north area of the basin. These anomalies consist of (1) low contents in Hf, Th, and U; (2) high contents in Sc, Co, and Zr; and (3) anomalous ratios in Th/Y, La/Tb, Ta/Y, and Ni/V. Basic supplies could be related to the alkaline volcanism during Norian-Hettangian and Aalenian-Bajocian times. Geochemical composition of rift deposits has been shown to be a useful and complementary tool to petrographic deduction in provenance, especially in intensely weathered sediments. However, diagenetic processes and hydrothermalism may affect the original detrital deposits, producing changes in geochemical composition that mislead provenance and weathering deductions.

Keywords: provenance, sandstones, geochemical composition, fluvial deposits, rift basins, Permian-Triassic, Jurassic, Early Cretaceous, Iberian Range.

INTRODUCTION

Studies in provenance have been mainly performed according to classic sandstone petrography. At present, several models are in common usage to deduce provenance parameters (source rock lithology, climate, weathering, transport, geotectonic setting) from petrographic analysis on sandstone framework (e.g., Basu et al., 1975; Dickinson and Suczek, 1979; Dickinson, 1985).

During the last two decades, the use of geochemical data for provenance inferences has experienced an important development (see McLennan et al., 1993), and models have been elaborated to decipher aspects concerning source lithology (Floyd and Leveridge, 1987; Gu et al., 2002), weathering (e.g., Nesbitt and Young, 1982; Taylor and McLennan, 1985), maturation during transport (Bhatia, 1983; Gu et al., 2002; Whitmore et al., 2004), and geotectonic setting (Bhatia and Taylor, 1981; Maynard et al.,

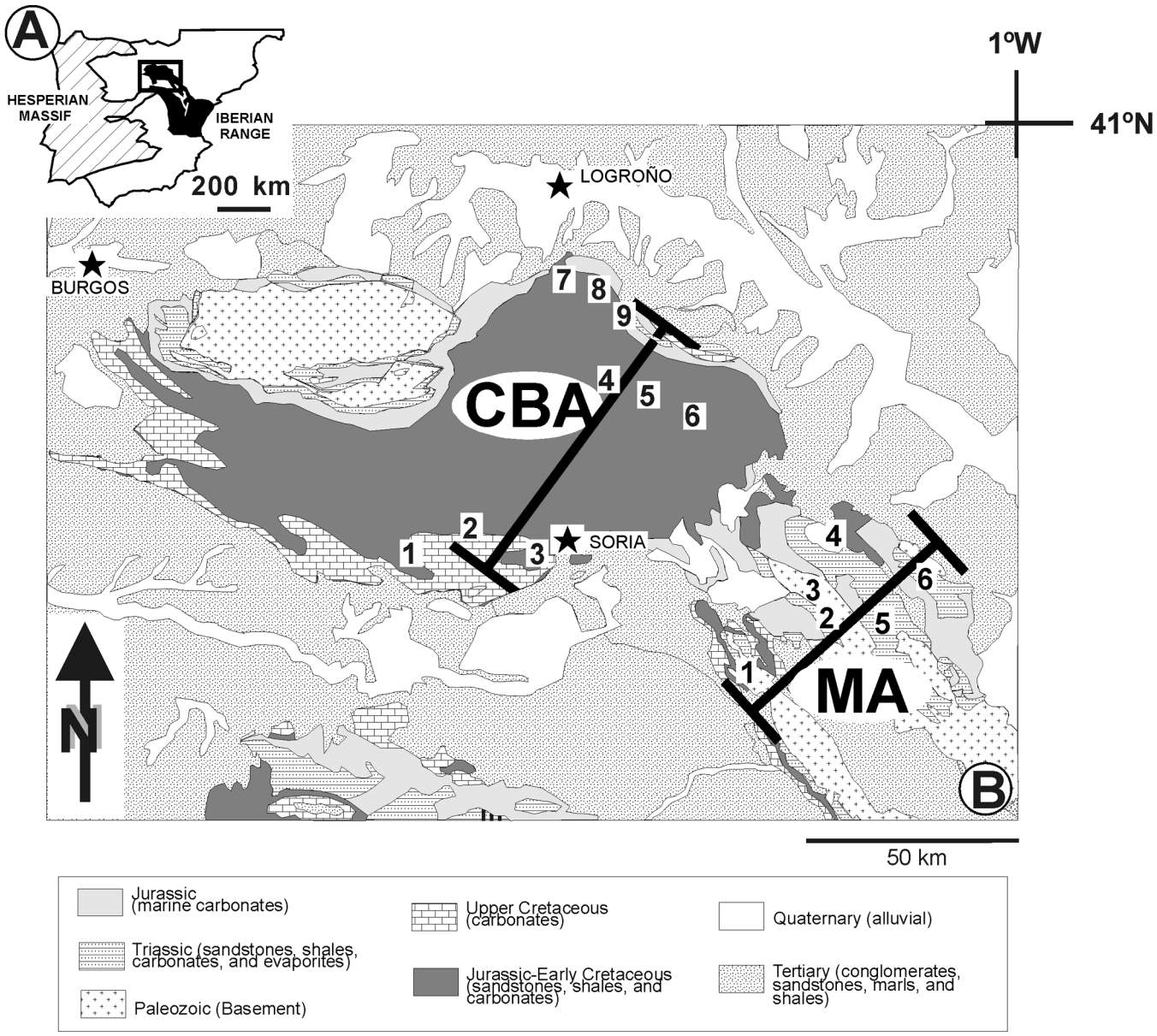

Figure 1. (A) Study area in the Iberian Peninsula. (B) Simplified geological map showing the location of sections in Permian-Triassic deposits on Moncayo area (MA): 1—Alameda section, 2—Aranda del Moncayo section, 3—Beratón section, 4—Moncayo section, 5—Tierga section, and 6—Tabuenca section; and the location of sections in Lower Cretaceous deposits on Cameros Basin area (CBA): 1—Muriel section, 2—Cidones-Abejar section, 3—Trinchera del Ferrocarril section, 4—Yanguas section, 5—San Pedro Manrique section, 6—Valdemadera section, 7—Trevijano section, 8—Jubera section, and 9—Arnedillo section.

1982; Bhatia, 1983, 1984; Roser and Korsch, 1985, 1986, 1988; Bhatia and Crook, 1986; McLennan and Taylor, 1991; Gu et al., 2002). Geochemical procedures generate quick and objective data, and they can be used on whole rock of clastic deposits from a wide range of grain sizes (Eynatten et al., 2003). In spite of these advantages, geochemical analysis may indicate a consistent loss of information about textures. Provenance origin of clasts (intrabasinal or extrabasinal, Zuffa, 1980; coeval or noncoeval, Zuffa, 1991) is indecipherable by whole-rock chemical analysis. In addition, diagenetic products are mixed with detrital material, and this fact may produce biased inferences on the provenance of original clastic material (García et al., 2004).

The Iberian Range is a linear structure trending NW-SE in the northeast edge of the Iberian microplate (Fig. 1); it is an intracratonic, folded segment of the Alpine Chain that developed as a rift basin (Iberian Basin) in two phases (e.g., Salas et al., 2001): the first phase was generated from the Early Permian to the Late Triassic, and the second phase of rifting occurred from Late Jurassic to early Albian time (Fig. 2). During these cycles, thick clastic sequences, from alluvial to lacustrine at the top, were deposited in grabens and half grabens. Both cycles evolved to periods of postrift thermal subsidence, where predominant shallow-marine carbonate sedimentation took place. During the Paleogene and Lower–Middle Miocene, compressive events caused structural inversion, folding, and thrusting.

Stratigraphy, sedimentology, and petrography of sediments generated during the two active rifting phases (Arribas, 1984; Arribas et al., 2003; Benito et al., 2001; Martín-Closas and Alonso-Millán, 1998; Mas et al., 2003; Ochoa et al., 2004) and the tectonic evolution of the basin (Guimerà et al., 1995; Salas

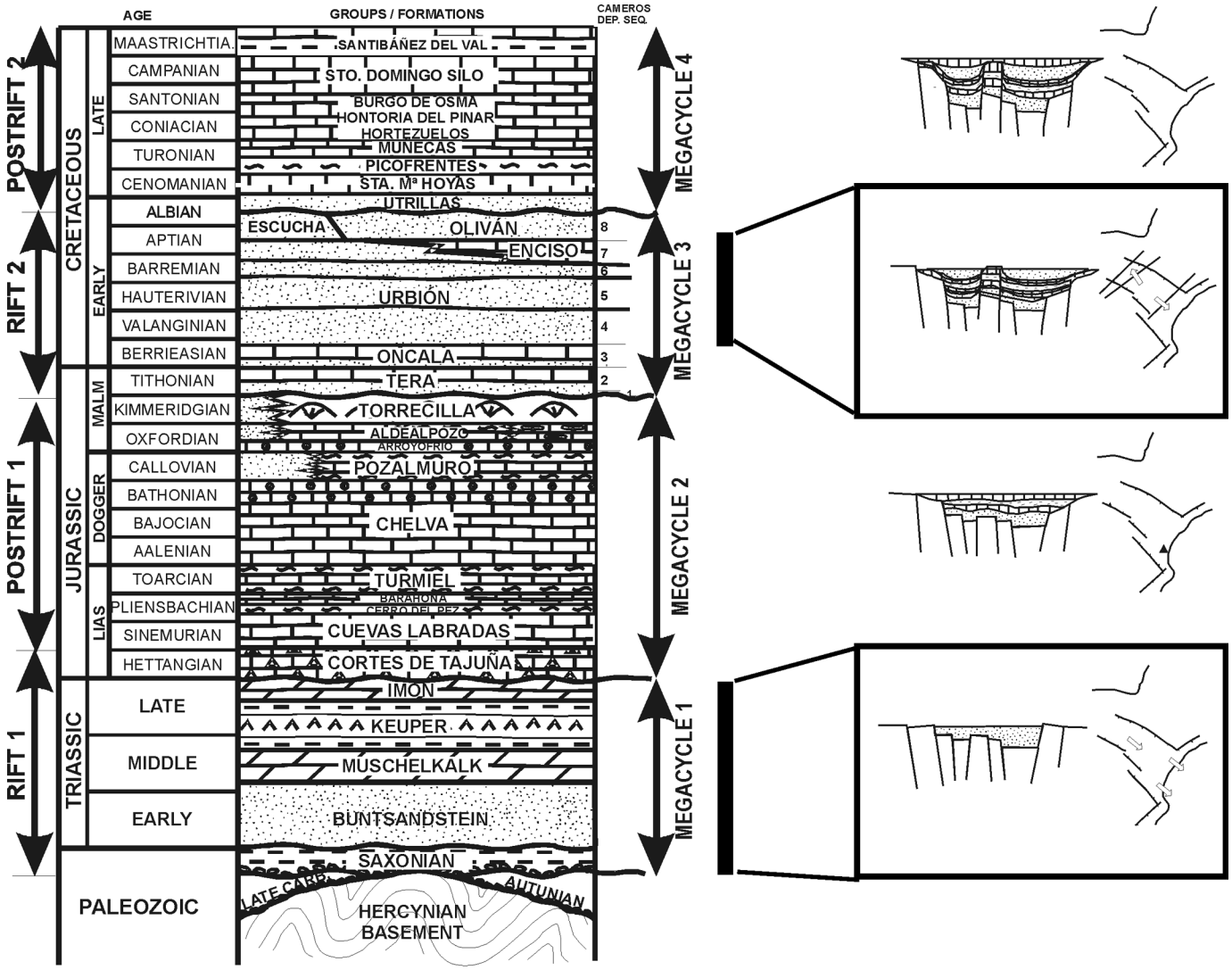

Figure 2. Synthetic sketches and stratigraphic section showing the stratigraphic record in the studied area and rift cycles on the evolution of the Iberian Basin (modified from Salas et al. [2001] and Mas et al. [2003]).

et al., 2001; Guimerà et al., 2004) have been consistently analyzed. Thus, these deposits represent an excellent opportunity to contrast geochemical data analysis with valuable background information.

The principal aim of this paper is to evaluate the informative power of geochemical data from petrographically well-known examples of clastic sediments generated at different times, but in a similar geotectonic scenario: the intracratonic Iberian Rift. Furthermore, the contrast of geochemical signatures between sediments generated during the two active stages of rifting may contribute to a better understanding of the evolution of the Iberian Rift. Finally, the data obtained in this paper will increase general knowledge of intracratonic rift basins and will be applicable to future models of such basin types.

GEOLOGICAL SETTING

The study area is located in the northwest sector of the Iberian Range in central Spain, and it includes clastic deposits from the first (Permian to Triassic) and second (Late Jurassic to Early Cretaceous) rifting stages. These deposits outcrop in two different areas: the Moncayo area, which is composed of Permian to Triassic deposits, and Cameros Basin, where Upper Jurassic to Lower Cretaceous deposits appear (Fig. 1).

During the Late Permian–Triassic extensional stage (rift 1, Fig. 2), the reactivation of the wrench faults as normal faults induced the propagation of rift systems in the Iberian plate as the Iberian Trough (Sopeña and Sánchez-Moya, 1997; Mas et al., 2003). This extensional stage corresponds to the beginning of the Alpine sedimentary cycle and is represented by the clastic Saxonian and Buntsandstein facies. These facies are continental clastic sediments that infilled asymmetrical half grabens (Fig. 3A). Buntsandstein deposits are mainly continental red beds that form the base of a sequence that evolve into siliciclastic and carbonate tidal sediments (Muschelkalk facies). The clastic infill in the Moncayo area consists mainly of arkosic deposits arranged into five main lithostratigraphic units (Arribas, 1984, 1985). The thickness of these deposits varies from 100 m to more than 900 m due to differential subsidence of troughs.

The second stage of rifting (Late Jurassic to Early Cretaceous) was related to the opening of the Central Atlantic (rift 2, Fig. 2). As a consequence, the Cameros Basin was formed as an extensional rift basin above a south-dipping ramp on a blind, low-angle normal fault several kilometers deep in the basement (Alonso and Mas, 1993; Guimerà et al., 1995; Salas et al., 2001). According to Alonso and Mas (1993) and Mas et al. (2003), the sedimentary record (Tithonian–early Albian) constitutes a large megasequence bounded by two main unconformities at the base and at the top, and it can be further subdivided into eight depositional sequences separated by minor unconformities (DS-1 to DS-8 in Fig. 2). This study is focused on the maximum synrift filling stage (DS-4 to DS-7 [late Berriasian to early Aptian]; Fig. 3B) related to maximum tectonic activity of this rifting phase. The infill of the basin varies drastically in thickness, from nearly 100 m in the marginal areas of the basin (toward NE and SW) to 2200 m in the depocentral areas (central sector) (Fig. 3B). This record is constituted by fluvial sequences that consist of coarse deposits of conglomerates and channelized fluvial (mainly braided) sandstone bodies in proximal areas evolving to meandering and lacustrine facies in distal areas (Mas et al., 2003; Ochoa et al., 2004). During the Middle to Late Cretaceous, a low-grade metamorphic event (hydrothermalism) took place in depocentral areas and affected the sedimentary record (Casquet et al., 1992; Barrenechea et al., 1995; Alonso-Azcárate et al., 1999).

METHODS

A total of 53 sandstone and shale samples was collected for geochemical analysis from several stratigraphic sections from both Permian-Triassic deposits in the Moncayo area (24 samples) and from Lower Cretaceous deposits (DS-4 to DS-7) in the Cameros Basin (29 samples). Sample locations are shown in Figure 3. Major and trace elements were determined for all samples. Analyses were performed at the Actlabs Laboratories (Canada) by Code 4Lithoresearch. All geochemical data are reported in Tables 1, 2, and 3.

For petrographic analysis of Permian-Triassic sandstones, one of the authors (J. Arribas) examined several databases from previous works (Arribas, 1984, 1987). This author provided thin sections of sandstones for analysis. For this paper, a new point counting method was performed on these samples following Gazzi-Dickinson criteria to obtain geotectonic inferences (Dickinson, 1985). In addition, Lower Cretaceous sandstones were analyzed petrographically following the same procedures and point-counting methods as those used for Permian-Triassic sandstones (Arribas et al., 2003; Ochoa et al., 2004).

RESULTS

Petrography

Permian and Triassic Sandstones

Framework composition of sandstones varies from quartzose (mean $Qm_{97}F_0Lt_3$; Qm—monocrystalline quartz; F—feldspars; Lt—total lithics) at the base of the succession (Saxonian facies; PS in Figs. 3A and 4A) to quartzofeldspathic (mean $Qm_{72}F_{25}Lt_3$) petrofacies at the top of the sedimentary sequence (Buntsandstein facies; B-1 and B-2 in Figs. 3A and 4A).

Quartzose Saxonian petrofacies (Fig. 5A) are very mature texturally; they show evidence of maturation during transport (very well-sorted sediments and high values of quartz grain roundness) and recycling of metasediments in the Variscan basement (e.g., presence of inherited quartz overgrowth). Lithic rock fragments are scarce and consist mainly of low-grade metamorphic fragments (shales and chert); some quartzose sandstone fragments also occur. Syntaxial quartz overgrowth is the main interstitial cement in the sandstones. Framework composition of Saxonian sandstones is very homogeneous in all the Moncayo

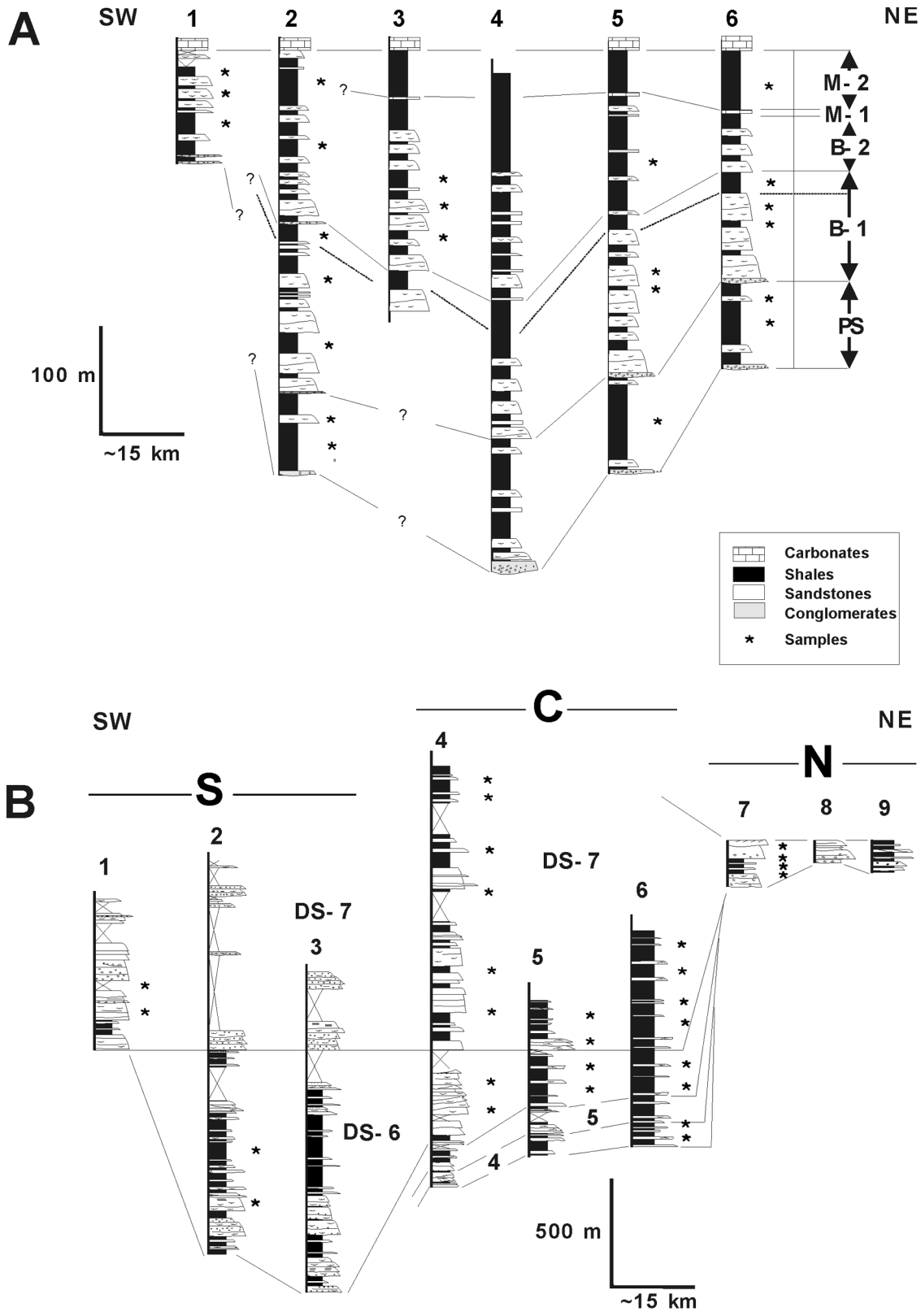

Figure 3. (A) SW-NE–trending stratigraphic correlation of analyzed sections in Permian-Triassic deposits in Moncayo area (MA, Fig. 1). Depositional sequences: PS—Saxonian facies; B-1 and B-2—Buntsandstein facies; M-1 and M-2—Muschelkalk facies. (B) Stratigraphic correlation of depositional sequences (from DS-4 to DS-7) in Lower Cretaceous sediments in Cameros Basin area (CBA, Fig. 1); S—southern area; C—central area; N—northern area. Note different vertical scales in A and B.

TABLE 1. MAJOR-ELEMENT COMPOSITION AND RELATED PARAMETERS FROM PERMIAN-TRIASSIC AND CRETACEOUS CLASTIC DEPOSITS IN THE NORTHWESTERN IBERIAN RANGE

Sample	Lithology†	SiO_2	Al_2O_3	Fe_2O_3	MnO	MgO	CaO	Na_2O	K_2O	TiO_2	P_2O_5	Fe_2O_3 + MgO	Al_2O_3/ SiO_2	Na_2O/ K_2O	SiO_2/ Al_2O_3	Fe_2O_3/ K_2O	CIA
Permian-Triassic (rift 1)																	
Tierga																	
BTL-1	sh	60.94	18.14	6.05	0.06	1.63	1.06	0.23	5.38	0.86	0.17	7.68	0.30	0.04	3.36	1.12	73.12
BTL-2	sh	58.43	19.93	7.64	0.03	2.25	0.39	0.28	5.84	0.81	0.17	9.89	0.34	0.05	2.93	1.31	75.38
BTL-3	sh	59.43	17.97	7.34	0.03	2.53	0.45	0.25	6.66	0.77	0.17	9.87	0.30	0.04	3.31	1.10	70.94
BTL-4	sh	51.98	20.19	8.24	0.03	4.42	0.46	0.25	6.96	0.71	0.19	12.66	0.39	0.04	2.57	1.18	72.47
BTA-1	ss	80.14	9.60	2.33	0.02	0.75	0.28	0.16	4.08	0.82	0.21	3.08	0.12	0.04	8.35	0.57	67.99
BTA-2	ss	76.49	10.44	2.94	0.02	1.14	0.59	0.21	4.82	0.92	0.21	4.08	0.14	0.04	7.33	0.61	65.01
Beraton																	
BBL-1	sh	58.17	20.25	7.54	0.02	1.88	0.29	0.29	6.57	0.94	0.19	9.42	0.35	0.04	2.87	1.15	73.91
BBL-2	sh	76.63	10.90	3.66	0.14	0.93	0.17	0.16	4.42	0.84	0.12	4.59	0.14	0.04	7.03	0.83	69.65
BBA-1	ss	78.38	10.88	1.51	0.01	0.64	0.15	0.17	5.81	0.59	0.14	2.15	0.14	0.03	7.20	0.26	63.96
Alameda																	
ALL-5	sh	57.86	16.96	6.35	0.07	3.00	1.67	0.26	5.18	0.86	0.22	9.35	0.29	0.05	3.41	1.23	70.46
ALL-11	sh	56.62	18.84	7.39	0.03	2.59	0.17	0.25	7.42	0.83	0.10	9.98	0.33	0.03	3.01	1.00	70.61
ALA-10	ss	57.85	6.19	1.41	0.13	0.28	16.05	0.17	4.64	0.06	0.06	1.69	0.11	0.04	9.35	0.30	22.88
Aranda																	
BRL-1	sh	74.95	10.96	4.94	0.06	0.81	0.70	0.14	3.32	0.85	0.14	5.75	0.15	0.04	6.84	1.49	72.49
BRL-2	sh	56.29	21.57	7.10	0.02	1.28	0.52	0.32	6.60	0.80	0.22	8.38	0.38	0.05	2.61	1.08	74.35
BRL-3	sh	64.26	16.06	5.62	0.04	1.34	1.12	0.21	4.99	0.88	0.17	6.96	0.25	0.04	4.00	1.13	71.76
BRL-3/R	sh	64.31	16.08	5.62	0.04	1.33	1.17	0.21	5.04	0.88	0.17	6.95	0.25	0.04	4.00	1.12	71.47
BRL-4	sh	73.51	8.88	2.89	0.09	1.15	3.38	0.16	3.80	0.87	0.17	4.04	0.12	0.04	8.28	0.76	54.75
BRL-5	sh	60.40	16.18	6.90	0.04	2.10	1.33	0.23	5.66	0.82	0.31	9.00	0.27	0.04	3.73	1.22	69.15
BRA-1	ss	89.47	4.62	1.93	0.04	0.32	0.14	0.09	1.48	0.46	0.09	2.25	0.05	0.06	19.37	1.30	72.99
BRA-2	ss	89.07	3.11	1.61	0.04	0.16	0.27	0.08	0.99	0.27	0.13	1.77	0.03	0.08	28.64	1.63	69.89
Tabuenca																	
BAL-1	sh	62.38	17.57	6.86	0.04	1.68	0.26	0.29	4.63	0.99	0.15	8.54	0.28	0.06	3.55	1.48	77.23
BAL-2	sh	64.30	16.44	6.35	0.04	2.18	0.47	0.23	4.82	0.90	0.16	8.53	0.26	0.05	3.91	1.32	74.86
BAL-3	sh	65.53	15.84	6.35	0.02	1.78	0.40	0.26	4.53	0.85	0.18	8.13	0.24	0.06	4.14	1.40	75.32
BAA-11	ss	88.82	4.49	1.55	0.11	0.54	0.82	0.11	1.50	0.24	0.10	2.09	0.05	0.07	19.78	1.03	64.88
Early Cretaceous (rift 2)																	
San Andrés																	
SAN-4	ss	92.97	2.46	2.04	0.13	0.20	0.40	0.10	0.21	0.38	0.04	2.59	0.03	0.03	0.48	9.71	77.60
Yanguas																	
YNG-L6	sh	57.43	23.91	6.44	0.02	0.86	0.30	1.30	3.80	1.04	0.08	23.93	0.42	0.42	0.34	1.69	81.58
YNG-L8	sh	56.14	23.56	8.19	0.04	0.93	0.26	1.24	3.14	1.04	0.10	23.60	0.42	0.42	0.39	2.61	83.55
YNG-L12	sh	78.35	10.86	3.45	0.04	0.54	0.50	0.68	1.44	0.93	0.06	10.90	0.14	0.14	0.47	2.40	80.56
YNG-L49	sh	55.76	25.75	6.76	0.07	0.49	0.12	0.75	4.16	0.85	0.06	25.82	0.46	0.46	0.18	1.63	83.66
YNG-6/R	ss	91.75	3.68	1.78	0.01	0.21	0.05	0.24	0.33	0.41	0.03	3.69	0.04	0.04	0.73	5.39	85.58
YNG-8	ss	96.27	1.86	0.93	0.01	0.09	0.04	0.14	0.12	0.20	0.03	1.87	0.02	0.02	1.17	7.75	86.11
YNG-12	ss	95.54	1.46	2.30	0.04	0.20	0.03	0.03	0.09	0.06	0.05	1.50	0.02	0.02	0.33	25.56	90.68
YNG-49	ss	88.82	5.83	1.98	0.01	0.26	0.10	0.45	0.85	0.36	0.06	5.84	0.07	0.07	0.53	2.33	80.64
San Pedro Manrique																	
SPM-3	ss	91.33	1.56	1.29	0.09	0.13	2.75	0.15	0.17	0.13	0.03	1.65	0.02	0.02	0.88	7.59	33.69
SPM-9	ss	89.68	5.52	1.13	0.02	0.14	0.26	0.44	0.79	0.78	0.05	5.54	0.06	0.06	0.56	1.43	78.74
SPM-15	ss	68.18	18.02	6.39	0.03	0.46	0.17	0.62	2.12	1.06	0.11	18.05	0.26	0.26	0.29	3.01	86.10
SPM-30	ss	89.96	3.97	3.68	0.02	0.65	0.03	0.10	0.42	0.52	0.04	3.99	0.04	0.04	0.24	8.76	87.83
Valdemadera																	
VLM-L2	sh	58.17	21.79	8.11	0.02	1.25	0.26	1.09	2.99	0.96	0.10	21.81	0.37	0.37	0.36	2.71	83.39
VLM-L7	sh	53.11	26.47	6.87	0.05	0.57	0.83	1.26	3.63	1.14	0.12	26.52	0.50	0.50	0.35	1.89	82.23
VLM-L11R	sh	69.22	17.91	4.16	0.09	0.31	0.08	0.78	2.56	1.08	0.08	18.00	0.26	0.26	0.30	1.63	83.97
VLM-L12	sh	61.13	20.74	6.57	0.05	0.73	0.19	0.71	3.61	0.89	0.11	20.79	0.34	0.34	0.20	1.82	82.14
VLM-2	ss	91.98	4.68	0.35	0.00	0.06	0.03	0.41	0.74	0.41	0.02	4.68	0.05	0.05	0.55	0.47	79.86
VLM-7	ss	91.94	4.20	1.55	0.01	0.21	0.08	0.34	0.43	0.45	0.05	4.21	0.05	0.05	0.79	3.60	83.17
VLM-11	ss	96.11	1.76	1.05	0.01	0.14	0.12	0.16	0.25	0.18	0.05	1.77	0.02	0.02	0.64	4.20	76.86
VLM-12	ss	61.13	20.72	6.53	0.05	0.73	0.20	0.75	3.62	0.90	0.11	20.77	0.34	0.34	0.21	1.80	81.93
Trevijano																	
TRE-L6	sh	29.74	9.45	3.45	0.07	0.79	27.25	0.07	2.15	0.45	0.06	4.37	0.32	0.32	3.15	1.60	24.28
TRE-L7	sh	33.54	8.38	3.16	0.04	0.64	26.84	0.05	1.89	0.43	0.06	4.94	0.25	0.25	4.00	1.67	22.55
TRE-5	ss	76.08	5.35	0.71	0.05	0.35	7.93	1.20	0.49	0.47	0.04	2.03	0.07	0.07	14.22	1.45	35.74
TRE-8	ss	62.76	0.95	0.77	0.02	0.22	19.31	0.16	0.11	0.21	0.02	3.50	0.02	0.02	66.06	7.00	4.63
Cidones																	
CID-33	sh	58.01	19.96	8.66	0.01	1.05	0.24	0.24	4.54	0.85	0.08	8.25	0.34	0.34	2.91	1.91	79.90
CID-31	ss	95.16	2.46	0.52	0.00	0.04	0.02	0.01	0.75	0.04	0.03	13.00	0.03	0.03	38.68	0.69	75.93
Gan																	
GAN-15	sh	59.56	23.62	2.49	0.01	0.81	0.04	0.30	4.60	1.09	0.05	3.07	0.40	0.40	2.52	0.54	82.70
GAN-13	ss	92.22	3.91	0.37	0.00	0.03	-0.01	0.03	1.55	0.22	0.04	12.33	0.04	0.04	23.59	0.24	71.35

Note: CIA—chemical index of alteration.
†ss—sandstones; sh—shales.

TABLE 2. TRACE-ELEMENT CONCENTRATIONS IN PPM AND RELATED PARAMETERS FROM PERMIAN-TRIASSIC AND CRETACEOUS CLASTIC DEPOSITS IN THE NORTHWESTERN IBERIAN RANGE

Sample	Lithology[†]	Th	U	Sc	Zr	Co[‡]	Hf	Rb	Cs	Ba	Sr	Y	Ta	Ni	V	K	La/Th	Co/Th	La/Sc	Th/Co	La/Co	Th/U
Permian-Triassic (rift 1)																						
Tierga																						
BTL-1	sh	16.56	3.66	17.00	213.81	6.06	6.46	180.00	18.98	597.47	148.81	31.40	1.46	21.00	94.00	24.03	2.64	0.37	2.57	2.73	7.21	4.52
BTL-2	sh	17.19	2.82	17.00	197.63	11.45	5.91	197.00	20.88	747.39	265.87	29.80	1.47	29.00	100.00	26.08	2.59	0.67	2.62	1.50	3.89	6.09
BTL-3	sh	16.67	4.09	15.00	206.16	13.65	6.27	203.00	19.65	707.42	86.37	30.30	1.57	29.00	92.00	29.74	2.45	0.82	2.72	1.22	2.99	4.08
BTL-4	sh	16.55	4.15	17.00	122.35	14.54	3.65	243.00	25.68	664.58	92.77	26.30	1.56	31.00	107.00	31.08	2.53	0.88	2.47	1.14	2.88	3.99
BTA-1	ss	13.49	2.66	4.00	273.33	4.12	7.66	130.00	8.31	297.90	55.72	26.00	1.34	–20.00	34.00	18.22	2.73	0.31	9.22	3.27	8.95	5.07
BTA-2	ss	14.27	2.57	6.00	275.41	5.25	7.51	129.00	8.30	341.19	80.45	27.50	1.40	–20.00	40.00	21.53	2.60	0.37	6.19	2.72	7.08	5.55
Beratón																						
BBL-1	sh	19.51	3.67	18.00	255.25	12.05	7.47	221.00	22.78	719.59	98.95	35.80	1.71	34.00	131.00	29.34	3.16	0.62	3.43	1.62	5.12	5.32
BBL-2	sh	15.73	3.67	8.00	434.94	9.67	12.41	125.00	10.96	457.96	38.57	33.30	1.46	–20.00	53.00	19.74	2.32	0.61	4.57	1.63	3.78	4.29
BBA-1	ss	9.93	1.91	3.00	234.43	2.45	6.49	146.00	6.62	386.45	41.37	19.00	0.99	–20.00	18.00	25.95	3.69	0.25	12.20	4.06	14.96	5.20
Alameda																						
ALL-5	sh	16.23	3.88	15.00	250.99	11.92	7.49	165.00	20.58	558.22	181.51	33.70	1.38	–20.00	76.00	23.13	3.32	0.73	3.59	1.36	4.52	4.18
ALL-11	sh	15.76	2.97	16.00	207.40	6.88	6.03	223.00	25.69	598.44	71.05	29.50	1.65	–20.00	85.00	33.14	3.31	0.44	3.26	2.29	7.58	5.30
ALA-10	ss	2.40	3.43	2.00	36.35	1.36	1.04	117.00	5.23	469.85	36.78	6.90	0.15	–20.00	9.00	20.72	3.48	0.57	4.18	1.76	6.15	0.70
Aranda																						
BRL-1	sh	14.64	3.64	10.00	365.25	4.68	10.52	126.00	13.17	446.09	91.72	35.80	1.38	–20.00	55.00	14.83	3.27	0.32	4.79	3.13	10.24	4.02
BRL-2	sh	16.12	3.14	19.00	160.29	5.19	4.79	238.00	31.02	746.91	385.47	27.90	1.49	–20.00	106.00	29.48	3.55	0.32	3.01	3.11	11.02	5.13
BRL-3	sh	14.42	3.17	14.00	247.14	7.86	7.27	172.00	18.89	558.38	200.36	32.40	1.39	20.00	81.00	22.29	3.38	0.55	3.49	1.83	6.21	4.55
BRL-3R	sh	14.34	3.16	14.00	242.10	7.91	7.14	170.00	18.39	568.77	201.86	32.70	1.33	–20.00	82.00	22.51	3.37	0.55	3.45	1.81	6.11	4.54
BRL-4	sh	15.98	3.54	6.00	525.61	6.68	14.69	111.00	8.11	864.14	90.70	35.30	1.55	–20.00	32.00	16.97	3.06	0.42	8.14	2.39	7.31	4.52
BRL-5	sh	16.11	3.68	13.00	273.60	8.77	7.87	198.00	22.50	544.90	184.54	35.50	1.55	–20.00	74.00	25.28	3.26	0.54	4.04	1.84	5.99	4.38
BRA-1	ss	9.12	2.31	3.00	438.26	1.44	12.07	50.00	3.23	1970.00	93.32	21.10	0.82	–20.00	27.00	6.61	3.81	0.16	11.58	6.32	24.04	3.95
BRA-2	ss	5.57	1.06	3.00	160.93	2.70	4.56	30.00	2.49	13,400.00	202.95	14.40	1.00	–20.00	16.00	4.42	3.45	0.49	6.41	2.06	7.11	5.26
Tabuenca																						
BAL-1	sh	15.87	3.81	16.00	282.62	10.68	8.02	169.00	13.85	519.94	160.98	36.00	1.53	21.00	110.00	20.68	3.43	0.67	3.40	1.49	5.10	4.17
BAL-2	sh	15.56	3.83	13.00	295.94	10.78	8.50	181.00	17.27	486.39	127.97	34.40	1.50	–20.00	89.00	21.53	3.41	0.69	4.08	1.44	4.92	4.06
BAL-3	sh	16.63	3.07	13.00	308.30	9.59	8.70	169.00	15.51	580.54	155.31	33.50	1.54	–20.00	98.00	20.23	2.87	0.58	3.67	1.73	4.98	5.42
BAA-11	ss	3.85	1.05	3.00	90.34	4.21	2.49	49.00	2.61	225.55	29.46	11.30	0.40	–20.00	20.00	6.70	3.86	1.09	4.95	0.92	3.53	3.67

(*continued.*)

TABLE 2. (*Continued.*)

Sample	Lithology[†]	Th	U	Sc	Zr	Co[‡]	Hf	Rb	Cs	Ba	Sr	Y	Ta	Ni	V	K	La/Th	Co/Th	La/Sc	Th/Co	La/Co	Th/U
Early Cretaceous (rift 2)																						
San Andrés																						
SAN-4	ss	3.61	1.19	1.00	153.09	6.00	4.21	10.20	0.73	27.19	14.07	8.76	0.62	–20.00	9.37	0.94	3.99	1.66	14.39	0.60	2.40	3.04
Yanguas																						
YNG-L6	sh	18.65	3.70	21.00	200.19	16.00	5.91	259.05	28.78	982.91	145.84	36.76	1.97	45.47	140.17	16.97	3.84	0.86	3.41	1.17	4.48	5.04
YNG-L8	sh	18.99	0.64	21.00	200.66	15.00	5.98	224.41	27.04	880.69	130.64	41.97	1.93	42.55	135.77	14.02	5.42	0.79	4.91	1.27	6.87	29.68
YNG-L12	sh	13.93	0.55	9.00	330.56	9.00	9.64	85.72	7.72	345.25	73.41	25.25	1.47	23.26	51.95	6.43	3.63	0.65	5.62	1.55	5.62	25.33
YNG-L49	sh	18.88	3.58	20.00	165.23	10.00	5.04	262.58	21.31	1450.00	87.71	31.03	1.78	21.29	118.47	18.58	3.07	0.53	2.90	1.89	5.79	5.27
YNG-6/R	ss	3.55	1.03	2.00	140.23	5.00	3.76	20.04	1.18	75.90	29.52	5.02	0.68	–20.00	20.42	1.47	4.43	1.41	7.86	0.71	3.14	3.44
YNG-8	ss	1.83	0.64	0.00	53.79	3.00	1.48	12.22	1.06	39.53	13.04	4.37	0.33	–20.00	9.37	0.54	4.75	1.64	0.00	0.61	2.89	2.85
YNG-12	ss	1.80	0.55	0.00	23.84	3.00	0.69	3.57	0.84	19.00	4.20	3.41	0.12	–20.00	8.51	0.40	2.87	1.66	0.00	0.60	1.73	3.28
YNG-49	ss	4.25	1.70	3.00	106.18	5.00	2.87	42.25	2.45	114.53	31.27	12.01	0.72	20.13	19.88	3.80	3.92	1.18	5.56	0.85	3.34	2.50
San Pedro Manrique																						
SPM-3	ss	1.53	0.53	0.00	35.97	3.00	1.03	5.56	0.65	30.19	15.94	4.55	0.26	–20.00	5.98	0.76	3.35	1.97	0.00	0.51	1.71	2.88
SPM-9	ss	8.07	1.90	4.00	269.79	2.00	7.43	45.86	2.28	187.37	41.88	17.40	1.10	–20.00	29.70	3.53	5.53	0.25	11.16	4.04	22.33	4.25
SPM-15	ss	16.65	3.97	17.00	268.26	2.00	8.14	142.78	10.76	506.12	67.51	47.90	1.84	30.03	98.33	9.47	3.05	0.12	2.99	8.33	25.40	4.20
SPM-30	ss	4.96	1.38	2.00	157.84	9.00	4.34	22.10	1.37	97.63	14.32	12.08	0.85	30.76	17.20	1.88	3.30	1.81	8.18	0.55	1.82	3.59
Valdemadera																						
VLM-L2	sh	16.65	2.49	19.00	189.59	15.00	5.81	192.89	23.00	595.00	202.00	36.30	1.73	57.84	117.17	13.35	1.66	0.90	1.46	1.11	1.85	6.69
VLM-L7	sh	22.03	3.25	23.00	183.70	10.00	5.73	225.35	26.00	684.00	224.00	34.65	2.34	27.49	136.67	16.21	2.28	0.45	2.18	2.20	5.01	6.78
VLM-L11R	sh	18.76	3.62	15.00	334.01	7.00	9.83	156.18	16.00	412.00	66.00	38.77	2.21	–20.00	85.25	11.43	2.13	0.37	2.66	2.68	5.70	5.18
VLM-L12	sh	20.01	6.90	17.00	246.62	16.00	7.49	211.95	16.00	788.00	109.00	41.05	1.83	44.86	105.56	16.12	2.44	0.80	2.87	1.25	3.05	2.90
VLM-2	ss	2.12	0.65	1.00	70.22	–1.00	1.88	43.95	2.70	118.38	60.52	4.39	0.69	–20.00	13.74	3.30	5.99	–0.47	12.71	-	3.05	3.26
VLM-7	ss	5.18	1.07	3.00	143.87	3.00	4.06	29.16	2.18	73.20	60.04	12.07	0.70	21.25	19.81	1.92	4.43	0.58	7.65	1.73	7.65	4.84
VLM-11	ss	1.59	0.54	1.00	34.84	2.00	0.98	10.49	0.75	24.79	17.05	3.00	0.34	–20.00	7.00	1.12	4.03	1.26	6.40	0.79	3.20	2.94
VLM-12	ss	19.99	6.88	17.00	245.54	15.00	7.43	209.03	15.47	858.01	107.30	40.73	1.87	45.17	102.65	16.17	2.42	0.75	2.85	1.33	3.23	2.91
Trevijano																						
TRE-L6	sh	7.52	2.06	9.00	98.13	4.79	3.07	135.00	12.50	133.20	245.77	25.28	0.89	30.29	121.79	9.60	5.28	0.64	4.42	1.57	8.30	3.65
TRE-L7	sh	7.52	2.11	8.00	122.52	2.50	3.68	121.00	13.24	170.54	170.11	27.35	0.97	23.74	107.35	8.44	5.00	0.33	4.70	3.01	15.04	3.56
TRE-5	ss	5.05	3.20	3.00	131.54	3.31	3.86	28.00	2.80	89.41	77.35	10.75	0.80	–20.00	26.88	2.19	3.75	0.66	6.32	1.53	5.73	1.58
TRE-8	ss	2.90	0.91	0.00	158.92	0.00	4.54	7.00	0.56	296.76	100.32	11.33	1.14	–20.00	6.68	0.49	5.14	0.00	0.00	-	6.73	3.19
Cidones																						
CID-33	sh	14.75	3.00	18.00	209.42	10.58	6.38	248.00	26.25	683.56	101.07	32.82	1.80	50.79	58.19	20.28	3.78	0.72	3.10	1.39	5.27	4.92
CID-31	ss	1.44	2.05	1.00	21.32	2.42	0.75	36.00	2.16	76.69	21.81	4.12	0.12	28.11	7.58	3.35	5.88	1.68	8.48	0.60	3.50	0.70
Gan																						
GAN-15	sh	16.40	3.72	20.00	258.64	11.10	7.73	242.00	29.01	770.45	98.46	38.66	2.46	29.65	62.03	20.54	3.31	0.68	2.72	1.48	4.90	4.41
GAN-13	ss	2.37	0.86	2.00	50.23	1.04	1.48	66.00	3.12	150.95	20.59	5.19	0.48	–20.00	6.85	6.92	4.98	0.44	5.89	2.28	11.34	2.75

[†]ss—sandstones; sh—shales.

[‡]Negative values indicate less than the reporting limit.

TABLE 3. RARE EARTH ELEMENT COMPOSITIONS AND RELATED PARAMETERS FROM PERMIAN-TRIASSIC AND CRETACEOUS CLASTIC DEPOSITS IN THE NORTHWESTERN IBERIAN RANGE

Sample	Lithology[†]	La	Ce	Pr	Nd	Sm	Eu	Gd	Tb	Dy	Ho	Er	Tm	Yb	Lu	REE[‡]	LREE	HREE	LREE/ HREE	La/Yb	$(La/Yb)_n$	$(La/Sm)_n$	$(Gd/Yb)_n$	Eu/Eu*
Permian-Triassic (rift 1)																								
Tierga																								
BTL-1	sh	43.70	85.02	9.38	35.38	7.24	1.49	6.20	1.01	5.68	1.13	3.17	0.51	3.31	0.49	203.71	180.72	21.50	8.40	13.18	8.91	3.80	1.52	0.68
BTL-2	sh	44.49	85.21	9.66	37.10	7.64	1.50	6.21	0.96	5.55	1.06	3.01	0.48	3.02	0.45	206.34	184.10	20.74	8.88	14.74	9.96	3.67	1.67	0.67
BTL-3	sh	40.86	78.53	8.72	32.77	6.81	1.33	5.66	0.97	5.50	1.07	2.98	0.47	2.99	0.45	189.13	167.69	20.11	8.34	13.65	9.22	3.78	1.53	0.66
BTL-4	sh	41.94	81.69	9.19	34.94	7.05	1.35	5.50	0.90	4.85	0.92	2.53	0.40	2.57	0.36	194.20	174.82	18.03	9.69	16.35	11.05	3.74	1.74	0.66
BTA-1	ss	36.87	72.85	7.91	30.07	6.20	0.97	5.11	0.86	4.84	0.92	2.52	0.40	2.59	0.37	172.47	153.90	17.60	8.74	14.25	9.63	3.74	1.60	0.53
BTA-2	ss	37.15	74.55	8.26	31.80	6.60	1.05	5.49	0.91	4.98	0.96	2.63	0.43	2.63	0.39	177.83	158.35	18.42	8.60	14.13	9.55	3.55	1.69	0.54
Beratón																								
BBL-1	sh	61.68	118.92	12.97	49.52	10.00	1.91	7.73	1.15	6.48	1.27	3.59	0.58	3.70	0.54	280.05	253.09	25.04	10.11	16.68	11.27	3.88	1.69	0.66
BBL-2	sh	36.56	71.60	7.83	30.32	6.54	1.15	6.10	1.04	6.02	1.17	3.35	0.54	3.51	0.55	176.27	152.84	22.28	6.86	10.41	7.03	3.52	1.41	0.55
BBA-1	ss	36.59	74.72	8.35	31.50	5.47	0.81	3.84	0.58	3.57	0.72	2.00	0.31	2.00	0.30	170.76	156.63	13.32	11.76	18.28	12.35	4.21	1.55	0.54
Alameda																								
ALL-5	sh	53.81	104.46	11.52	43.69	8.77	1.77	7.47	1.16	6.75	1.30	3.55	0.55	3.63	0.53	248.96	222.25	24.94	8.91	14.84	10.03	3.86	1.67	0.67
ALL-11	sh	52.18	104.76	12.12	45.89	8.96	1.74	7.08	1.01	5.78	1.10	3.04	0.47	3.01	0.46	247.58	223.90	21.94	10.20	17.35	11.72	3.66	1.91	0.67
ALA-10	ss	8.36	16.52	1.93	7.15	1.61	0.38	1.44	0.22	1.22	0.23	0.62	0.10	0.62	0.08	40.48	35.57	4.53	7.86	13.55	9.16	3.27	1.89	0.77
Aranda																								
BRL-1	sh	47.92	95.01	10.45	39.91	7.95	1.53	7.17	1.13	6.66	1.33	3.66	0.58	3.75	0.57	227.61	201.24	24.84	8.10	12.78	8.63	3.80	1.55	0.62
BRL-2	sh	57.16	113.28	12.24	45.70	9.11	1.92	7.38	1.06	5.69	1.08	2.94	0.45	2.92	0.44	261.37	237.49	21.96	10.82	19.56	13.22	3.95	2.05	0.72
BRL-3	sh	48.80	94.93	10.51	39.05	7.89	1.59	6.89	1.06	6.12	1.23	3.38	0.54	3.44	0.53	225.97	201.18	23.20	8.67	14.20	9.60	3.89	1.63	0.66
BRL-3R	sh	48.35	93.39	10.28	38.69	7.79	1.59	6.90	1.05	6.22	1.23	3.37	0.52	3.43	0.52	223.35	198.51	23.25	8.54	14.09	9.52	3.91	1.63	0.66
BRL-4	sh	48.84	96.79	10.82	40.82	8.28	1.33	7.47	1.12	6.66	1.30	3.65	0.59	3.75	0.57	231.99	205.54	25.11	8.19	13.01	8.79	3.71	1.61	0.52
BRL-5	sh	52.49	101.20	11.24	42.64	8.80	1.83	7.82	1.18	6.90	1.31	3.49	0.54	3.46	0.52	243.42	216.37	25.22	8.58	15.17	10.25	3.75	1.83	0.67
BRA-1	ss	34.73	69.39	7.43	27.59	5.31	0.95	4.31	0.64	3.89	0.78	2.17	0.35	2.26	0.36	160.17	144.45	14.76	9.79	15.39	10.40	4.12	1.55	0.61
BRA-2	ss	19.22	39.27	4.23	16.04	3.40	0.56	3.19	0.49	2.75	0.52	1.41	0.21	1.31	0.20	92.81	82.16	10.08	8.15	14.62	9.88	3.55	1.97	0.52
Tabuenca																								
BAL-1	sh	54.46	106.77	11.82	44.37	8.98	1.79	7.78	1.15	6.60	1.34	3.65	0.57	3.72	0.56	253.56	226.39	25.38	8.92	14.62	9.88	3.82	1.69	0.66
BAL-2	sh	53.02	107.51	11.56	43.44	8.48	1.64	6.93	1.07	6.27	1.27	3.49	0.57	3.60	0.55	249.40	224.02	23.75	9.43	14.72	9.95	3.93	1.56	0.65
BAL-3	sh	47.75	92.65	10.10	37.32	7.29	1.44	6.39	1.02	6.01	1.17	3.26	0.53	3.46	0.52	218.93	195.11	22.37	8.72	13.80	9.33	4.12	1.50	0.65
BAA-11	ss	14.84	30.34	3.39	13.18	2.74	0.60	2.64	0.40	2.18	0.42	1.10	0.17	1.10	0.16	73.24	64.48	8.17	7.90	13.44	9.08	3.42	1.94	0.68

(*continued*.)

TABLE 3. (*Continued*.)

Sample	Lithology[†]	La	Ce	Pr	Nd	Sm	Eu	Gd	Tb	Dy	Ho	Er	Tm	Yb	Lu	REE[‡]	LREE	HREE	LREE/ HREE	La/Yb	$(La/Yb)_n$	$(La/Sm)_n$	$(Gd/Yb)_n$	Eu/Eu*
Early Cretaceous (rift 2)																								
San Andrés																								
SAN-4	ss	14.39	29.75	3.24	12.54	2.57	0.53	2.13	0.31	1.66	0.31	0.90	0.15	0.95	0.14	69.59	62.50	6.57	9.52	15.15	10.15	3.47	1.82	0.70
Yanguas																								
YNG-L6	sh	71.69	140.95	15.69	60.43	12.60	2.47	9.76	1.35	7.01	1.32	3.60	0.59	3.64	0.52	331.62	301.36	27.79	10.84	19.68	13.18	3.53	2.17	0.69
YNG-L8	sh	103.01	200.81	21.50	82.55	16.20	2.72	11.33	1.58	8.16	1.47	4.03	0.64	3.90	0.57	458.45	424.07	31.66	13.40	26.42	17.70	3.94	2.35	0.62
YNG-L12	sh	50.61	95.12	10.25	38.08	7.38	1.18	5.58	0.84	4.76	0.94	2.69	0.44	2.84	0.43	221.14	201.44	18.52	10.88	17.81	11.93	4.25	1.59	0.57
YNG-L49	sh	57.92	109.94	12.08	44.56	8.71	1.84	7.03	1.08	5.96	1.13	3.16	0.51	3.21	0.47	257.59	233.21	22.54	10.35	18.06	12.10	4.12	1.77	0.73
YNG-6/R	ss	15.71	28.10	3.14	11.75	2.17	0.32	1.48	0.16	0.89	0.18	0.55	0.09	0.62	0.10	65.26	60.87	4.07	14.97	25.23	16.90	4.50	1.92	0.55
YNG-8	ss	8.68	16.82	1.83	6.98	1.35	0.23	1.03	0.15	0.77	0.15	0.43	0.07	0.41	0.06	38.95	35.65	3.07	11.59	21.05	14.10	3.99	2.03	0.60
YNG-12	ss	5.18	10.89	1.20	4.45	1.02	0.26	0.73	0.11	0.62	0.12	0.32	0.05	0.30	0.04	25.28	22.73	2.29	9.93	17.24	11.55	3.16	1.97	0.93
YNG-49	ss	16.69	31.67	3.34	12.51	2.55	0.49	2.52	0.42	2.31	0.45	1.24	0.20	1.19	0.17	75.77	66.77	8.51	7.85	14.01	9.39	4.05	1.72	0.60
San Pedro Manrique																								
SPM-3	ss	5.12	10.83	1.25	5.04	1.19	0.22	1.10	0.17	0.89	0.16	0.42	0.06	0.40	0.05	26.91	23.43	3.26	7.19	12.82	8.59	2.66	2.23	0.59
SPM-9	ss	44.66	86.42	9.38	35.29	6.50	1.08	4.26	0.59	3.18	0.62	1.74	0.28	1.79	0.27	196.04	182.24	12.72	14.33	24.94	16.71	4.26	1.93	0.64
SPM-15	ss	50.81	97.01	10.88	41.86	8.91	2.23	8.35	1.47	8.39	1.65	4.57	0.73	4.37	0.65	241.88	209.47	30.18	6.94	11.63	7.79	3.54	1.55	0.80
SPM-30	ss	16.37	32.25	3.40	12.82	2.67	0.45	2.27	0.39	2.15	0.44	1.20	0.20	1.23	0.19	76.05	67.52	8.07	8.36	13.26	8.88	3.80	1.49	0.57
Valdemadera																								
VLM-L2	sh	27.71	51.67	5.50	20.89	4.69	1.13	5.38	1.08	6.77	1.36	3.75	0.61	3.76	0.54	134.84	110.45	23.26	4.75	7.37	4.94	3.66	1.16	0.70
VLM-L7	sh	50.13	95.90	10.43	39.51	7.71	1.25	6.49	1.11	6.55	1.30	3.59	0.58	3.68	0.54	228.78	203.68	23.85	8.54	13.62	9.13	4.03	1.43	0.55
VLM-L11R	sh	39.87	79.42	8.66	32.76	6.44	1.08	5.98	1.10	6.58	1.34	3.86	0.64	4.08	0.62	192.42	167.15	24.20	6.91	9.76	6.54	3.84	1.19	0.54
VLM-L12	sh	48.75	94.45	10.35	38.63	8.14	1.69	7.45	1.28	7.38	1.41	3.93	0.63	3.99	0.58	228.67	200.33	26.65	7.52	12.21	8.18	3.71	1.51	0.67
VLM-2	ss	12.71	25.00	2.82	10.52	1.80	0.33	1.19	0.16	0.84	0.16	0.45	0.07	0.48	0.07	56.59	52.84	3.41	15.48	26.36	17.66	4.38	2.00	0.70
VLM-7	ss	22.96	46.47	5.18	19.56	3.61	0.47	2.79	0.41	2.31	0.44	1.23	0.19	1.18	0.17	106.97	97.78	8.73	11.20	19.38	12.99	3.94	1.91	0.45
VLM-11	ss	6.40	13.01	1.43	5.65	1.21	0.22	0.84	0.13	0.64	0.12	0.31	0.05	0.31	0.04	30.37	27.70	2.45	11.33	20.53	13.75	3.28	2.19	0.67
VLM-12	ss	48.46	93.62	10.10	38.69	8.14	1.66	7.33	1.28	7.31	1.45	3.97	0.62	3.98	0.58	227.19	199.01	26.52	7.50	12.18	8.16	3.69	1.49	0.67
Trevijano																								
TRE-L6	sh	39.75	53.72	7.51	31.42	5.98	1.16	5.08	0.82	4.05	0.81	2.45	0.33	2.10	0.28	155.46	138.38	15.91	8.70	18.97	12.82	4.18	1.96	0.09
TRE-L7	sh	37.60	52.25	7.17	30.10	5.82	1.15	5.07	0.81	4.09	0.84	2.56	0.35	2.25	0.30	150.38	132.95	16.28	8.17	16.72	11.30	4.06	1.83	0.09
TRE-5	ss	18.96	33.78	4.03	17.01	3.32	0.60	2.62	0.42	2.08	0.40	1.22	0.18	1.08	0.16	85.86	77.10	8.16	9.45	17.62	11.91	3.59	1.98	0.09
TRE-8	ss	14.93	21.88	2.99	12.30	2.21	0.36	2.00	0.33	1.73	0.35	1.11	0.16	1.00	0.14	61.51	54.31	6.83	7.95	14.95	10.11	4.26	1.63	0.09
Cidones																								
CID-33	sh	55.77	100.04	11.78	47.86	9.00	1.74	7.36	1.25	6.25	1.25	4.00	0.56	3.73	0.50	251.08	224.45	24.89	9.02	14.97	10.11	3.90	1.60	0.09
CID-31	ss	8.48	14.06	1.84	7.78	1.62	0.33	1.25	0.17	0.87	0.17	0.51	0.07	0.50	0.07	37.70	33.77	3.60	9.38	17.12	11.57	3.29	2.04	0.09
Gan																								
GAN-15	sh	54.36	95.91	11.20	45.41	8.70	1.74	7.45	1.36	7.33	1.47	4.59	0.66	4.37	0.57	245.13	215.59	27.81	7.75	12.45	8.41	3.93	1.38	0.09
GAN-13	ss	11.77	23.84	2.94	12.48	2.50	0.50	1.62	0.24	1.11	0.21	0.66	0.09	0.65	0.09	58.70	53.52	4.68	11.44	18.16	12.27	2.97	2.03	0.09

[†]ss—sandstones, sh—shales.

[‡]Rare earth element (REE) chondrite-normalizing factors are from Taylor and McLennan (1985); REE = La-Lu; light (L) REE = La-Sm; heavy (H) REE = Gd-Lu.

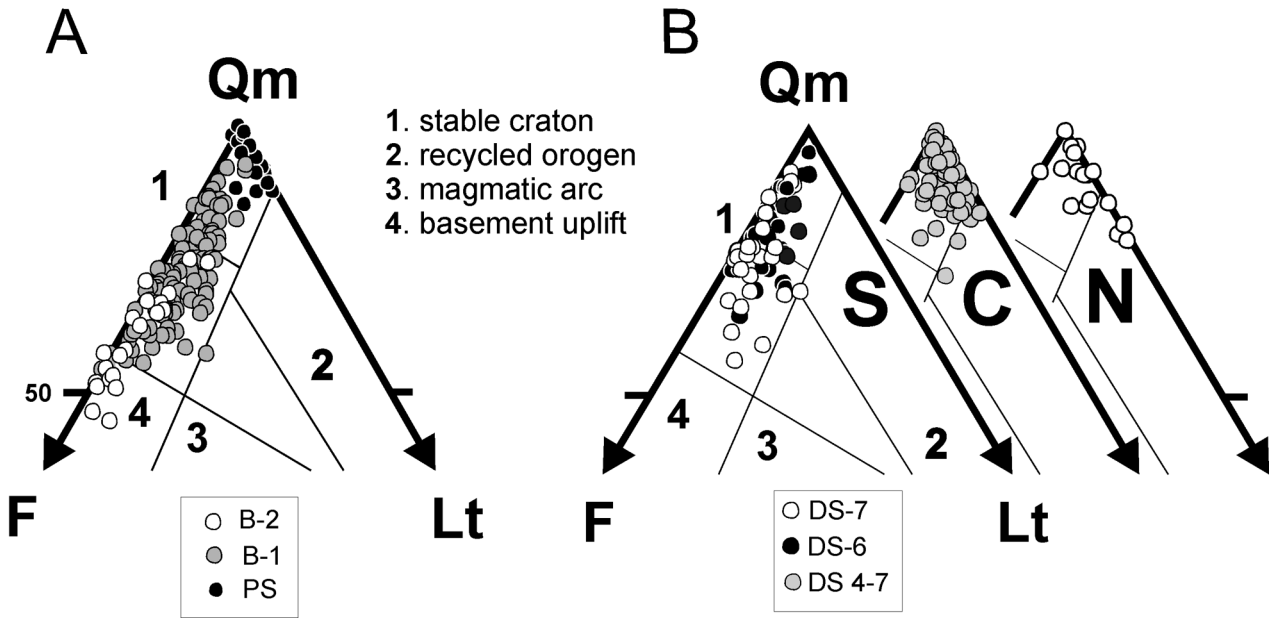

Figure 4. (A) QmFLt ternary plot (Dickinson, 1985) showing the evolution of petrofacies in Permian-Triassic sandstones. (B) QmFLt ternary plots (Dickinson, 1985) showing the variations of Berriasian to Lower Aptian petrofacies throughout the basin. PS—Saxonian facies; B-1 and B-2—Buntsandstein facies; DS-4 to DS-7—depositional sequences in Lower Cretaceous sediments.

area. These sandstone petrofacies represent the initial stage of rift 1, when metasedimentary cover was eroded.

Sandstone composition of Buntsandstein facies represents a drastic change from the provenance of underlying sediments. Quartzofeldspathic petrofacies suggest that the contribution of coarse crystalline rocks from the Hesperian Massif (Fig. 1A) diluted the supplies from metasedimentary rocks (Arribas et al., 1985). The content of feldspar varies, showing a consistent increase of K-feldspar to the top (Figs. 4A and 5B). The presence of these K-feldspar–rich petrofacies may suggest both arid conditions of Buntsandstein sedimentation (Arribas, 1984) and nearness to source area. Syntaxial K-feldspar and quartz overgrowths and minor carbonate are the main interstitial cements. Matrix is constituted by illite and minor kaolinite minerals and is mainly of diagenetic origin: epimatrix (alteration of K-feldspars), pseudomatrix (lithic rock fragment disaggregration), kaolinite pore-filling and illite pore-lining (Arribas, 1987).

Cretaceous Sandstones

The sandstone framework composition of depositional sequences 4, 5, 6, and 7 is very quartzose, with variable amounts of K-feldspar and lithics (Fig. 4B). In proximal areas (sections 1, 2, and 3 from CBA in Figs. 1 and 3), sandstone composition is quartzofeldspathic (mean $Qm_{81}F_{18}Lt_1$; S in Figs. 4B and 5C), and it evolves to more mature quartzose sandstones in depocentral areas (mean $Qm_{96}F_3Lt_1$; C in Figs. 4B and 5D). This fact suggests an important maturation during transport (~50 km) in humid climate (Rat, 1982). Quartzofeldspathic petrofacies are indicative of a plutoniclastic origin from coarse crystalline sources from the Hesperian Massif (Arribas et al., 2003). In addition, in the northeast edge of the basin, local supplies from Triassic and Jurassic sedimentary rocks (carbonate and clastics) produce quartzolithic sandstones petrofacies (mean $Qm_{93}F_1Lt_6$; N in Fig. 4B). Framework replacements by carbonate and kaolinite on K-feldspars have been identified. In addition, few metamorphic lithic grains were crushed producing pseudomatrix. As mentioned earlier, a low-grade metamorphic event (hydrothermalism) took place in depocentral areas of the basin, provoking some mineralogical changes in original sands. Some of these changes are silicification and chloritization of feldspars, metamorphic lithic grains, and intrabasinal argillaceous grains, as well as the growth of chloritoid crystals on these deposits (Barrenechea et al., 1995; Alonso-Azcárate et al., 1999; Mantilla-Figueroa, 1999).

Geochemical Composition

Major Elements

Major-element compositions of the shales and sandstones with derived geochemical parameters and indices are given in Table 1. Absolute concentrations in the different major elements (expressed in oxides) are higher in shales than in sandstones, except for SiO_2 (Table 1; Fig. 6).

Sandstones show an intermediate to high content in SiO_2, generally between 76.49% and 89.47% in Permian-Triassic (rift 1) sandstones and between 61.13% and 96.27% in Lower Cretaceous (rift 2) sandstones, and both can be considered as mature sandstones (Pettijohn et al., 1973). In some cases the SiO_2 content is extraordinarily low (57.85%, sample ALA–10, Table 1) due to pervasive carbonate cementation. In comparison, shales show a typical intermediate content in SiO_2 (between 51.98%

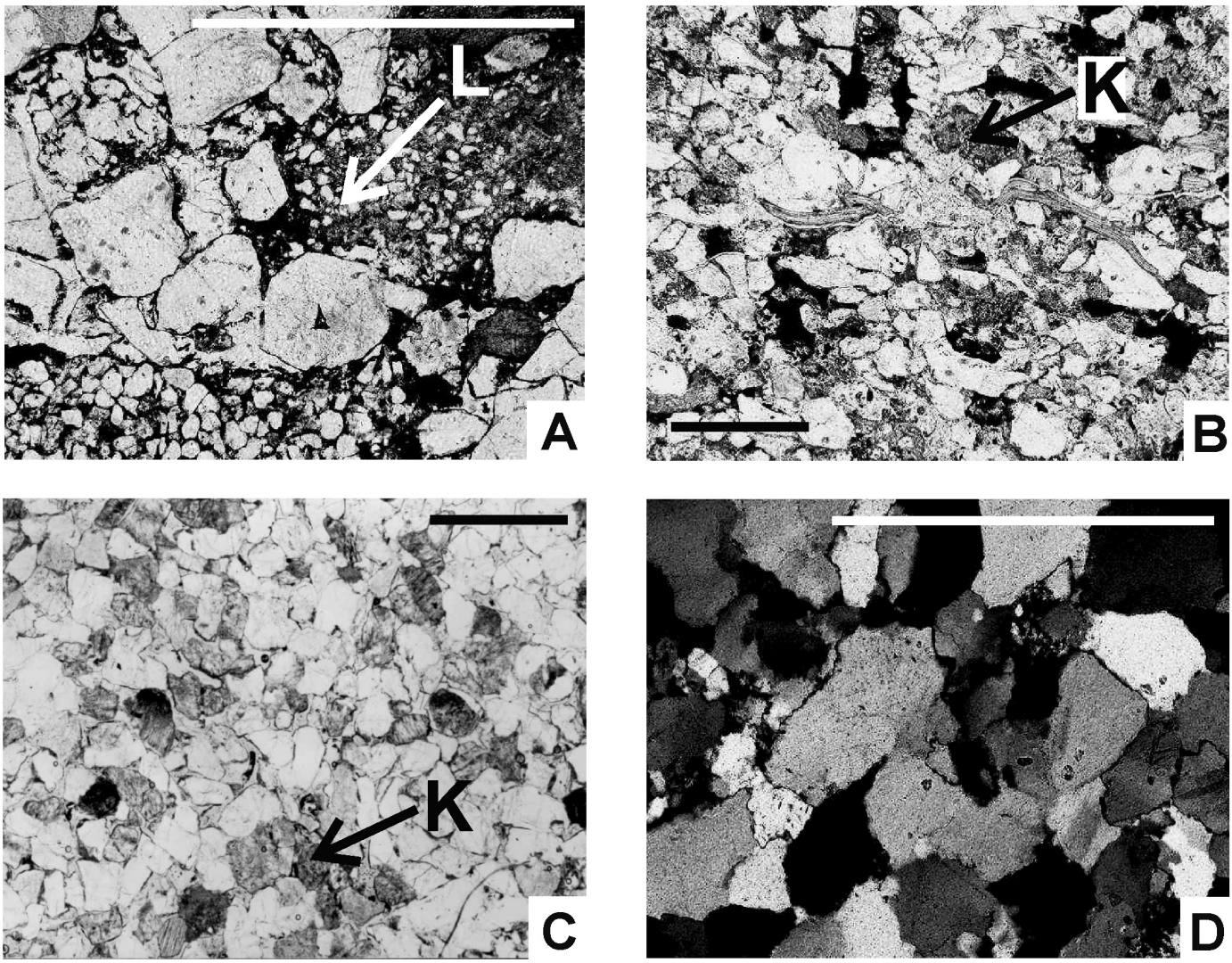

Figure 5. Microphotographs showing general aspects of petrofacies from Permian-Triassic and Lower Cretaceous sandstones. (A) Quartzolithic petrofacies of Saxonian sandstones. L—sedimentary lithic fragment. Parallel nichols. (B) Quartzofeldspathic petrofacies of Buntsandstein sandstones. K—K-feldspar. Parallel nichols. (C) Quartzofeldspathic petrofacies of Lower Cretaceous sandstones from southern zone of the basin. K—K-feldspar. Parallel nichols. (D) Quartzose petrofacies of Lower Cretaceous sandstones from center zone of the basin. Crossed nichols. Scale bars = 1 mm.

and 76.63% in rift 1 shales and between 29.74% and 78.35% in rift 2 shales).

Both shales and sandstones have an intermediate Al_2O_3/SiO_2 ratio (0.03–0.39 in rift 1 deposits and 0.02–0.50 in rift 2 deposits). This ratio in sandstones (0.09 in rift 1 sandstones and 0.06 in rift 2 sandstones) shows values lower than shales (0.27 and 0.35 in rift 1 and rift 2, respectively). The high clay minerals content in shales is reflected by a high percentage in Al_2O_3 (8.88%–21.57% in rift 1 shales and between 8.38% and 26.47% in rift 2 shales; Table 1). Lower values in Fe_2O_3 + MgO are found in sandstones (1.69–4.08, mean 2.44 in rift 1; 1.50–20.77, mean 6.53 in rift 2) while shale values are higher (4.04–12.66, mean 8.22 in rift 1; 3.07–26.52, mean 16 in rift 2).

Harker diagrams for SiO_2 versus Al_2O_3 show a negative correlation (Fig. 6). Other negative correlations can be observed between SiO_2 versus Fe_2O_3, K_2O, MgO, Na_2O, and TiO_2. Nevertheless, marked positive correlations exist for Al_2O_3 versus K_2O (correlation coefficient r = 0.86 and 0.95 in rift 1 and rift 2 deposits), Al_2O_3 versus MgO (correlation coefficient r = 0.77 and 0.76 in rift 1 and rift 2 deposits), and Al_2O_3 versus TiO_2 (correlation coefficient r = 0.69 and 0.90 in rift 1 and rift 2 deposits) (Fig. 6).

CaO and MnO versus SiO_2 do not present a clear correlation. A CaO-SiO_2 scatter could result from carbonate cementation during diagenesis (Gu et al., 2002). Most samples present low CaO percentages (<1 wt%), though in some cases (ALA-10 sample, Table 1), high content is observed (near 16 wt%) due to the presence of carbonate cement. On the other hand, Al_2O_3

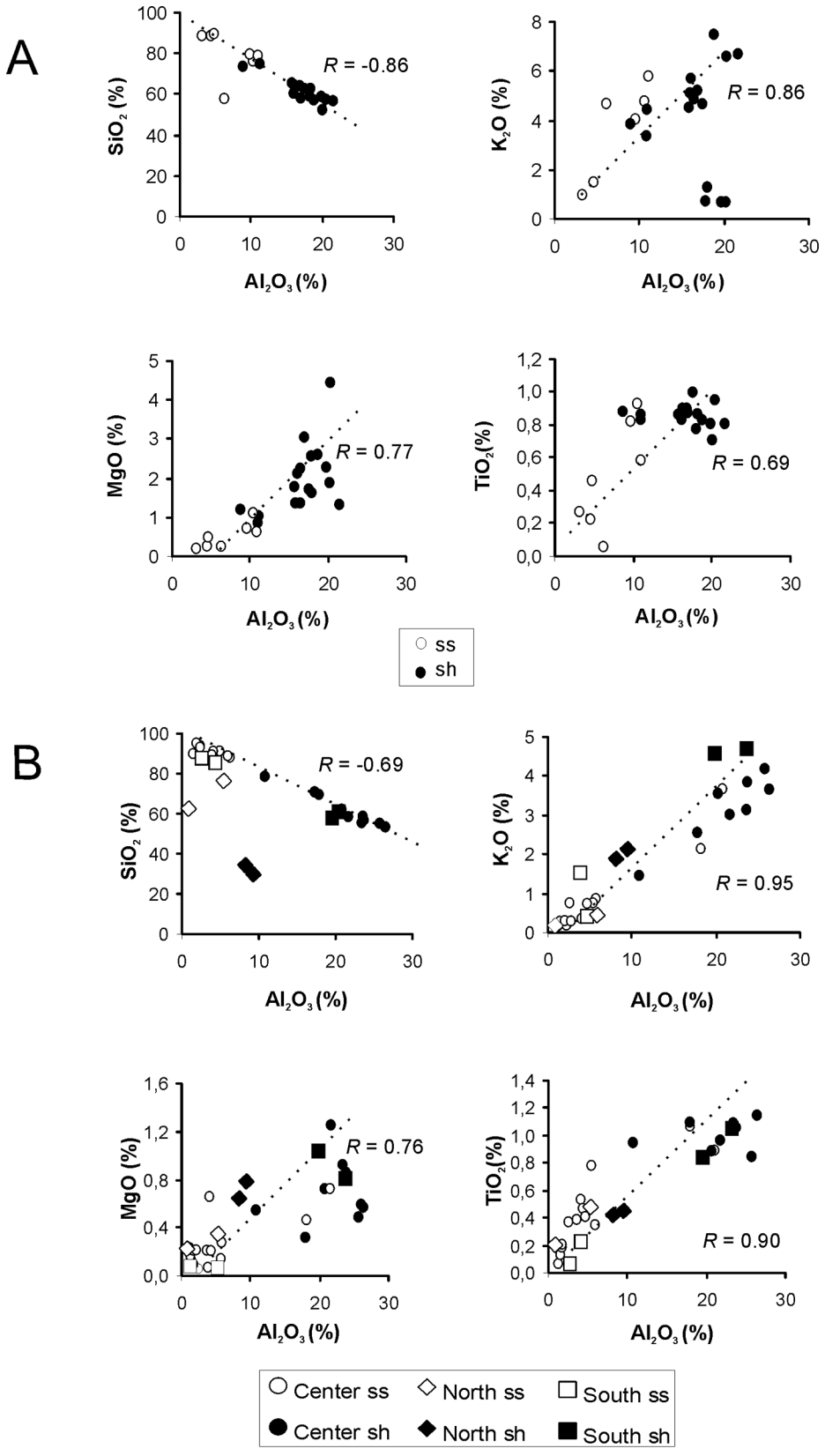

Figure 6. Harker diagrams showing major-element variation for both zones. (A) Permian-Triassic deposits, and (B) Lower Cretaceous deposits. Data are from Table 1; ss—sandstones, sh—shales.

versus CaO presents a negative correlation (correlation coefficient $r = -0.30$ and -0.18 in rift 1 and rift 2 deposits) in shales because Ca is leached during chemical weathering (Nesbitt et al., 1980).

Large Ion Lithophile Elements (LILEs)

The contents of Rb (30–242, mean 156 ppm in rift 1 deposits; 3–262, mean 106 ppm in rift 2 deposits), Cs (30–119, mean 15 ppm in rift 1 deposits; 0.60–29, mean 10 ppm in rift 2 deposits), Ba (25–13, mean 1144 ppm in rift 1 deposits; 19–1450, mean 368 ppm in rift 2 deposits), and Sr (29–385, mean 130 ppm in rift 1 deposits; 4–246, mean 81 ppm in rift 2 deposits) show a considerable scatter (Table 2), but their average values are comparable with the North American shale composite (NASC) (Gromet et al., 1984) or Average Upper Crust (AUC) (Taylor and McLennan, 1981). On the whole, shales display higher Rb, Cs, Ba, and Sr contents than sandstones.

Positive correlations are observed in K versus Rb (correlation coefficient $r = 0.31$ and 0.97 in rift 1 deposits and rift 2 deposits, respectively), K versus Sr (correlation coefficient $r = 0.31$ and 0.38 in rift 1 deposits and rift 2 deposits, respectively), K versus Cs (correlation coefficient $r = 0.25$ and 0.90 in rift 1 deposits and rift 2 deposits, respectively), and K versus Ba (correlation coefficient $r = 0.31$ and 0.78 in rift 1 deposits and rift 2 deposits, respectively). This suggests that K-rich clay minerals (such as illite) control the presence of these trace elements (McLennan et al., 1983; Feng and Kerrich, 1990). Sr content is low in rift 1 and rift 2 deposits, which would imply that the source rocks were poor in plagioclase (Feng and Kerrich, 1990).

Rare Earth Elements (REEs)

In Table 3, REE compositions are shown for shales and sandstones in each stratigraphic section. La to Lu elements were considered to determine absolute concentrations and several characteristic parameters (ΣREE, ΣLREE, ΣHREE, ΣLREE/ΣHREE, Eu/Eu*, La/Yb, La/Sm, Gd/Yb, where L is light and H is heavy.).

Samples generally show uniform and similar values to the NASC (Gromet et al., 1984) and the AUC (Taylor and McLennan, 1981). The most significant signatures are: (1) high LREE (La to Sm), (2) moderate HREE (Gd to Lu), and (3) a negative Eu anomaly. Values for shales are slightly higher than for sandstones, as seen in the chondrite-normalized REE diagrams (Fig. 7). The general tendency between sandstones and shales and among all the stratigraphic sections is very similar in all diagrams.

The enrichment in LREE in both rift 1 and rift 2 deposits is reflected by a high ratio of $(La/Yb)_n$ (7.03–13.22, mean 9.93 and between 4.94 and 17.70, mean 11.34, respectively), $(La/Sm)_n$ (3.27–4.21, mean 3.78 and 2.66–4.50, mean 3.79, respectively), and ΣLREE/HREE (6.86–11.76, mean 8.92 and 6.94–15.48, mean 9.70, respectively). A significant negative Eu anomaly (Eu/Eu*) is marked in the diagrams with values between 0.52 and 0.77, mean 0.63, in rift 1 deposits and 0.09–0.93, mean 0.49, in rift 2 deposits.

DISCUSSION

Weathering of the Source Area

The positive correlations between Al_2O_3 versus K_2O, Al_2O_3 versus MgO, and Al_2O_3 versus TiO_2 (Fig. 6) indicate that weathering was an important control in the source area in rift 1 and rift 2 deposits (Feng and Kerrich, 1990). Al and Ti are stable or residual elements during chemical weathering, while K and Mg are fixed in the clay minerals and Ca is leached (Nesbitt et al., 1980). Sandstones and shales in rift 1 and rift 2 deposits show variable degrees of negative correlations for SiO_2 versus Al_2O_3 related to the increase of mineralogical maturity (Bhatia, 1983;

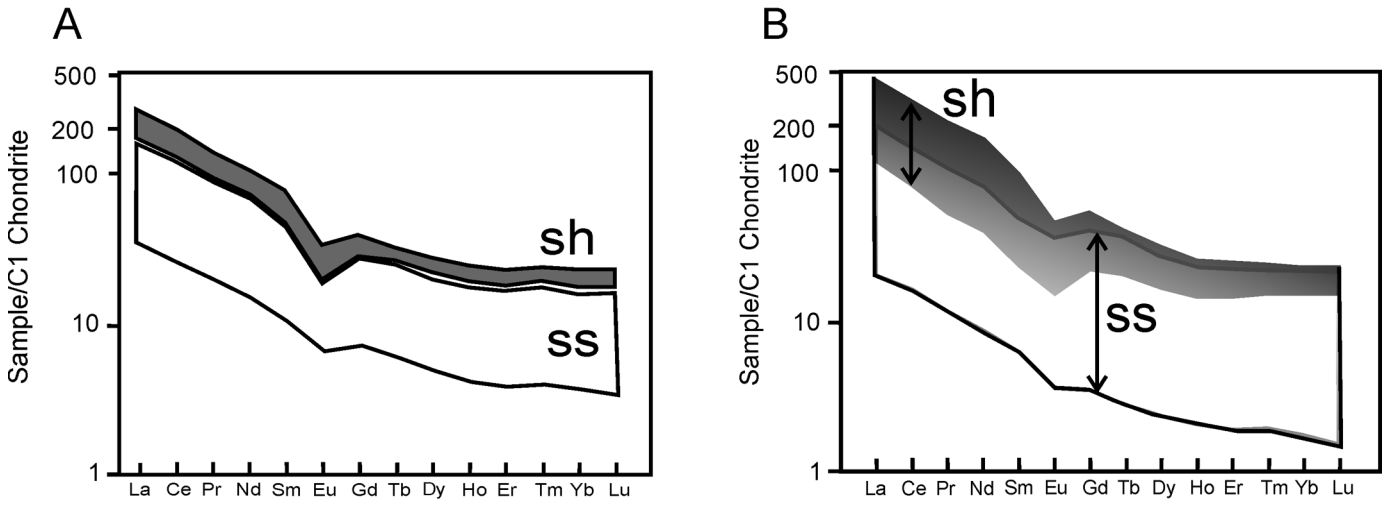

Figure 7. Chondrite-normalized rare earth element (REE) diagram showing interval values from shales and sandstones from (A) Permian-Triassic deposits and (B) Lower Cretaceous deposits. Data are from Table 2. Chondrite-normalizing values are from Taylor and McLennan (1985); ss—sandstones, sh—shales.

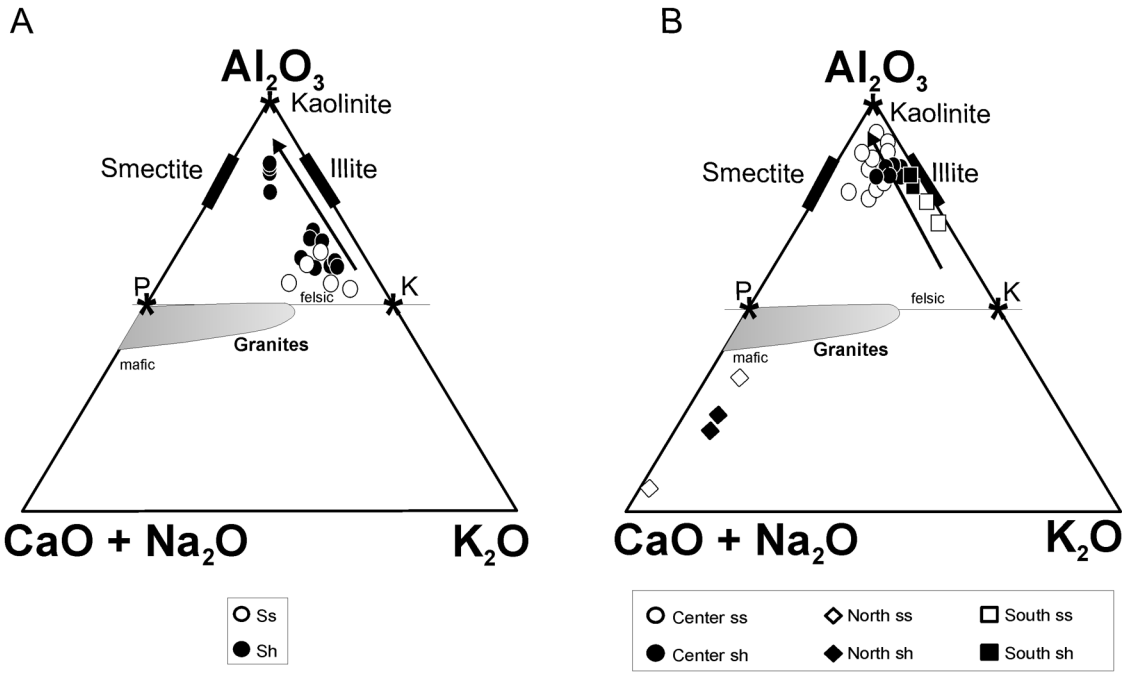

Figure 8. Chemical index of alteration (CIA) ternary plots of molecular proportions Al_2O_3-(Na_2O + CaO)-K_2O showing the weathering trend in (A) Permian-Triassic deposits and (B) Lower Cretaceous deposits. P—plagioclase; K—K-feldspar (after Nesbitt and Young, 1982); ss—sandstones; sh—shales.

Gu et al., 2002). These data are supported by the petrographic observations (Fig. 5).

The positive correlations between K versus Ba, K versus Rb, and K versus Cs indicate a clear relationship with alteration of minerals enriched in K (McLennan et al., 1983; Feng and Kerrich, 1990). Illite is enriched in K and Al, and as a consequence, an increase in illite corresponds to a greater abundance of Al, K, and their positively correlated elements.

The chemical index of alteration (CIA) of Nesbitt and Young (1982) was calculated to estimate the degree of weathering of source rocks (Table 1; Fig. 8). Values for sandstones vary between 63 and 73 in rift 1. Values in rift 2 sandstones are generally higher (71–91). These CIA values are according to petrographic compositional data from both rift sediments (Fig. 5). A better preservation of K-feldspar during the Triassic is observed. This fact may reflect a more intense weathering during Early Cretaceous (rift 2) than in Triassic (rift 1) times, as a consequence of climate conditions (Rat, 1982).

Rift 1 shales present higher CIA values than sandstones (70–78), suggesting that the main weathering products concentrate in shales as clay minerals. Graphic expression of the CIA suggests that weathering produces the alteration of K-feldspar to clay minerals as illite (Fig. 8A). Lower values in rift 1 sandstones can be explained as an intermediate value between those estimated for the unweathered source area (idealized value for granites, see Fig. 8A) and the shales values, outlining the weathering sequence.

CIA values of rift 2 sandstones are extremely high and plot near rift 2 shales (Fig. 8B), probably due to humid climate during sedimentation of rift 2 deposits (Rat, 1982).

In spite of these observations, the presence of hydrothermal chlorite minerals in rift 2 deposits could have increased the content of Al_2O_3 and biased interpretations about weathering (Grigsby, 2001). In addition, diagenetic alteration of K-feldspars (epimatrix) in rift 1 and rift 2 sandstones (Arribas, 1987; Mata, 1997) would increase the illite content in sandstones and thus increases in Al_2O_3 and CIA values can be expected.

Anomalous values consisting of high CaO + Na_2O content are detectable in some rift 2 sandstones in the northern area of Cameros Basin (TRE-8, TRE-5, and SPM-3; Table 1; Fig. 8B). This can be explained by the nature of source rock (Triassic and Jurassic sedimentary carbonates) and interstitial carbonate cements (Ochoa et al., 2004). Furthermore, sedimentary provenance for samples in this area produces supplies with low contents in siliciclastic minerals.

Several authors (Taylor and McLennan, 1985; McLennan et al., 1995; Gu et al., 2002) have used the Th/U ratio to decipher the weathering history due to the oxidation and loss of uranium during the weathering process. Sediments of rift 1 deposits show a cluster slightly above the upper crust value, with a short weathering trend in shales (arrows in Fig. 9A). This could mean that weathering conditions were constant during Permian-Triassic sedimentation. On the other hand, rift 2 sandstones display anomalous low ratios of Th/U with low Th and U contents, and

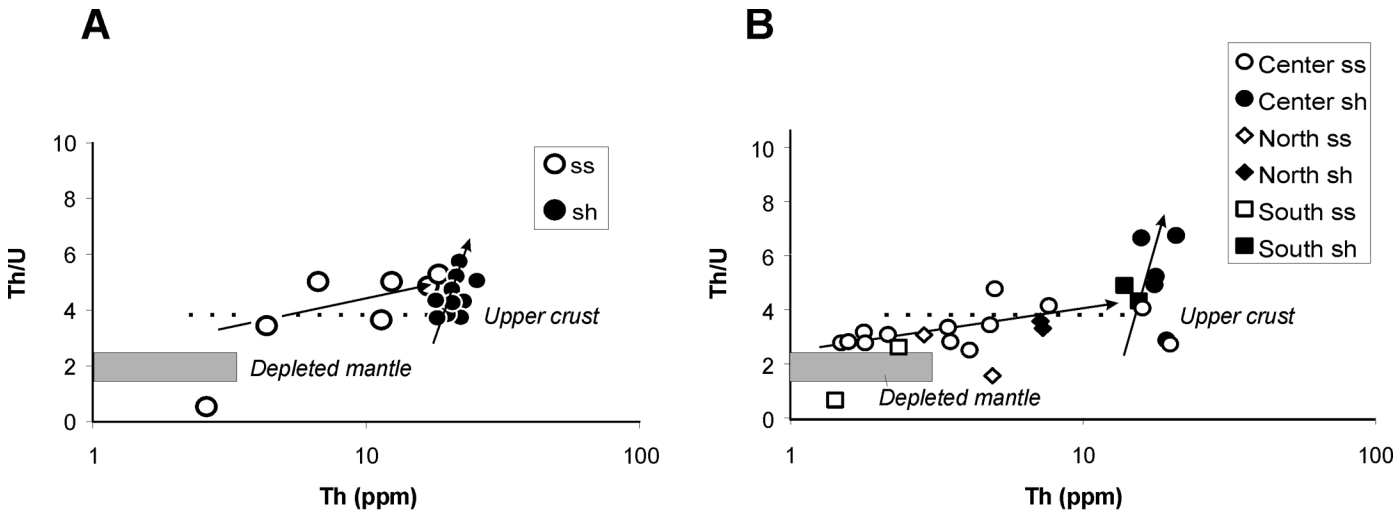

Figure 9. Elemental ratio Th/U and Th abundances (Taylor and McLennan, 1985) in (A) Permian-Triassic deposits and (B) Lower Cretaceous deposits. Arrows show weathering trends in sandstones (ss) and shales (sh).

they plot below the upper crust mean value (Fig. 9B). These anomalies could be related to provenance imprints, and probably to a coarser-grained texture in some samples that produces an important decrease of Th-rich dense minerals, as discussed next. Additionally, weathering trends in rift 2 sandstones and shales are visible and correspond to more intense weathering (higher values of Th/U ratios) than in Permian-Triassic deposits.

Tectonic Setting and Nature of Source Rocks

Using major elements, Bhatia (1983) and Roser and Korsch (1986) determined broad tectonic settings: oceanic and continental island arcs, and active and passive continental margins. According to these authors, both rift 1 and rift 2 deposits plot in or near the passive continental margin field (Fig. 10). Intracratonic grabens (aulacogens, e.g., Iberian Basin) are similar to passive-margin settings in terms of the nature of the crust (Bhatia and Crook, 1986).

Trace elements such as La, Th, Sc, Co, and Zr are transferred into clastic sediments during primary weathering, due to their low mobility. Thus, they are useful tools for provenance and tectonic discrimination (Bhatia, 1985; Taylor and McLennan, 1985; McLennan and Taylor, 1991; Bhatia and Crook, 1986; Gu et al., 2002).

We used La-Th-Sc, Th-Co-Zr/10, and Th-Sc-Zr/10 discrimination plots of Bhatia and Crook (1986) to characterize the tectonic setting (Fig. 11). In the La-Th-Sc ternary diagram, rift 1 and rift 2 samples plot in the field defined by Bhatia and Crook (1986) for graywackes from continental margins. However, no discrimination between passive and active continental margins can be observed in this diagram. Shales show a higher content in Sc than sandstones due to the increase in clay minerals where this element is fixed (Mata et al., 2000). In Th-Sc-Zr/10 and Th-Co-Zr/10 ternary plots, rift 1 and 2 sandstones plot mainly in the continental passive-margin field (Bhatia and Crook, 1986), but shales and some rift 2 sandstones plot in the continental island-arc field. This fact is again possibly due to the higher content of Sc in clay minerals. In addition, rift 2 sandstones from the central and northern area of the Cameros Basin show high contents in Zr and Co. The high contents in Zr could be associated with sorting and maturation processes during transport (McLennan et al., 1993; García et al., 2004; Whitmore et al., 2004). High content in Co can be related to provenance, as will be discussed in the following sections.

In rift 1 and 2 deposits, enrichment in LREEs, the characteristic negative Eu anomalies, and the flat HREE patterns suggest derivation from an old upper continental crust composed chiefly of felsic components (Gu et al., 2002).

Floyd and Leveridge (1987) proposed the La/Th versus Hf diagram to discriminate between different source compositions. Most rift 1 and 2 samples plot in the felsic source field (Fig. 12). However, low contents in Hf in some rift 2 samples force them to be plotted in the andesitic field (Fig. 12B).

La/Co average ratios are 10.25 and 6.63 for rift 1 and 2 sandstones, respectively (Table 2). On the other hand, Th/Co average ratios are 3.02 and 1.67 for rift 1 and 2 samples, respectively (Table 2; Fig. 13). Sands derived from granitoid sources show higher La/Co and Th/Co values than those sands derived from basaltic sources (Cullers and Berendsen, 1998). Rift 1 and rift 2 sandstones plot in an average range corresponding to sediments derived from upper continental crust.

All these general inferences about tectonic setting and nature of source rocks using minor elements in rift 1 and rift 2 deposits agree with an upper continental crust main provenance. However, some important anomalies are observed specially in some Cretaceous sandstone from the central and northern area of the basin. These anomalies are: (1) high content in Sc, Co, and Zr; (2) low content in Hf, Th, and U, and (3) anomalies in ratios like

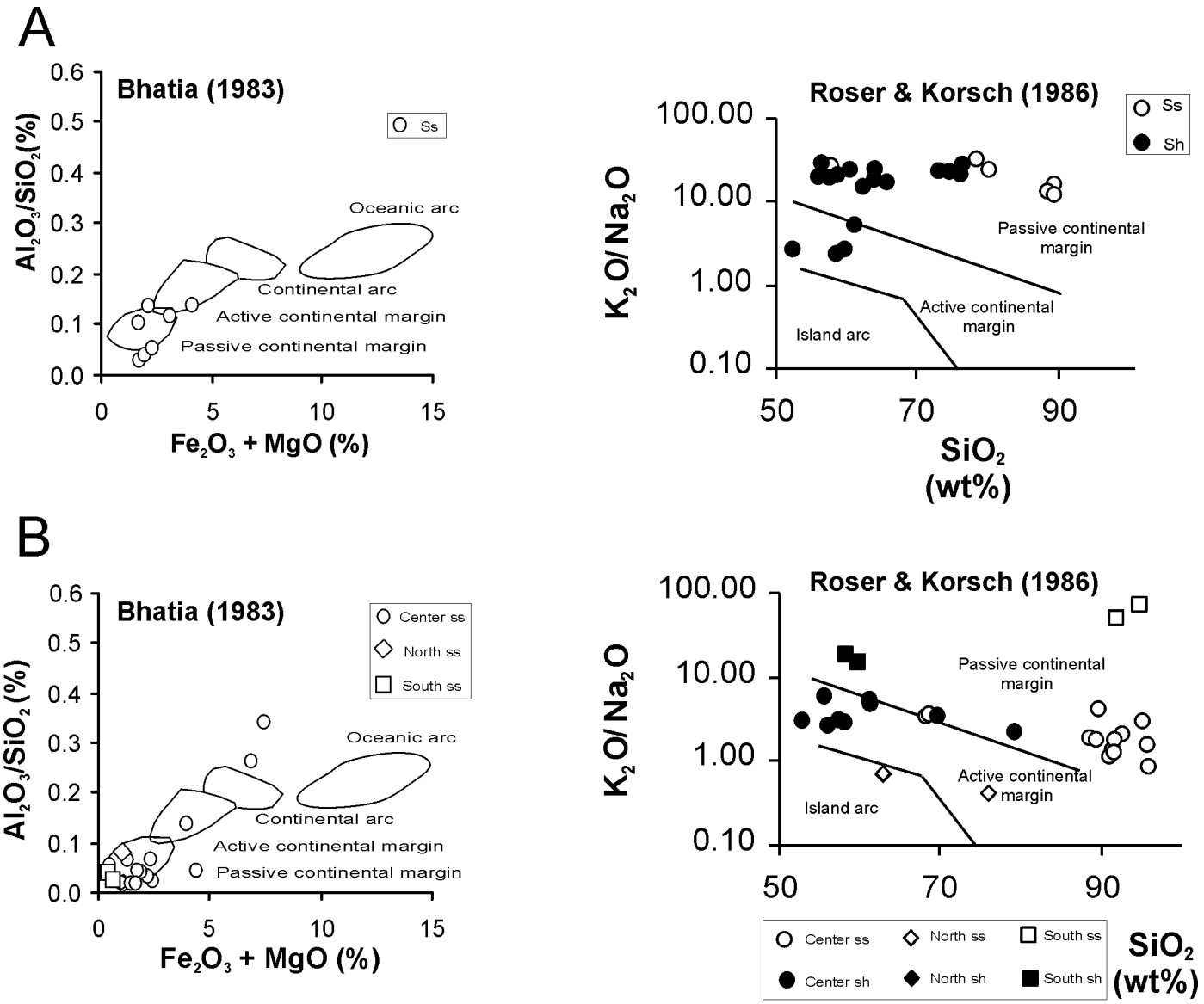

Figure 10. Tectonic-setting discrimination diagrams (ss—sandstones, sh—shales) for Permian-Triassic (A) and Lower Cretaceous samples (B).

Th/Y (mean 2.9), La/Tb (mean 35.53), Ta/Y (mean 1.11), and Ni/V (mean 0.72). These data produce important shifts in diagnostic provenance diagrams to intermediate-basic source fields (e.g., continental island arc, Bhatia and Crook, 1986; andesitic source, Floyd and Leveridge, 1987; basalt, Cullers and Berendsen, 1998). However, a clear compositional elemental spectrum that characterizes basic sources is observed, suggesting a mixture of a main felsic source with minor contribution from a mafic source (e.g., alkaline intermediate magmatism). The mafic sources must be considered in relation with a post-Buntsandstein magmatic activity, because these anomalies are not observed in the Triassic deposits (rift 1). Along the northern and southern margins of the Iberian Rift system, and during Norian to Bajocian times, several episodes of basaltic volcanic activity occurred (Salas and Casas, 1993; Martínez-González et al., 1996; Salas et al., 2001; González Menéndez and Suárez, 2005).

The presence of anomalous samples in the northern and central area of the Cameros Basin suggests that basic sources could be associated with Triassic and Jurassic sedimentary rocks located to the north of this basin that acted as sources during Early Cretaceous times.

In summary, petrography and geochemical data suggest that during the first stage of rifting (Permian-Triassic) sources were related to felsic coarse-grained rocks, associated with upper continental crust provenance (Hesperian Massif). In the second stage of rifting, during the most active phase (Berriasian–early Aptian), felsic upper crust provenance was maintained and located in the SW part of the basin (Arribas et al., 2003). In addition, in the NE

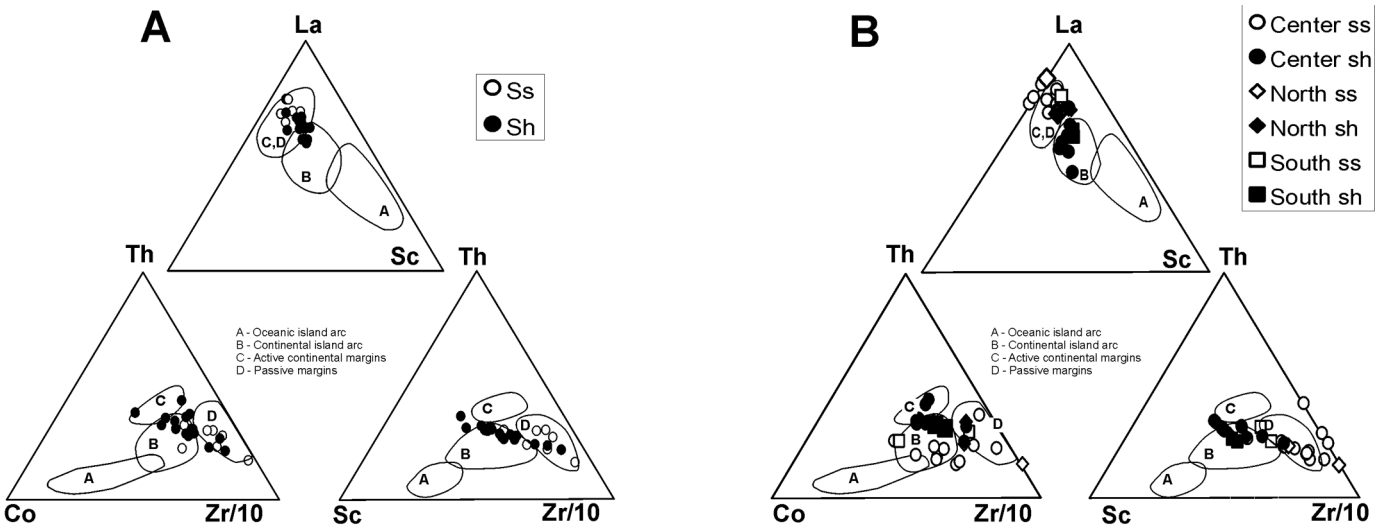

Figure 11. Tectonic-setting discrimination diagrams (ss—sandstones, sh—shales) (Bhatia and Crook, 1986) for Permian-Triassic (A) and Lower Cretaceous samples (B).

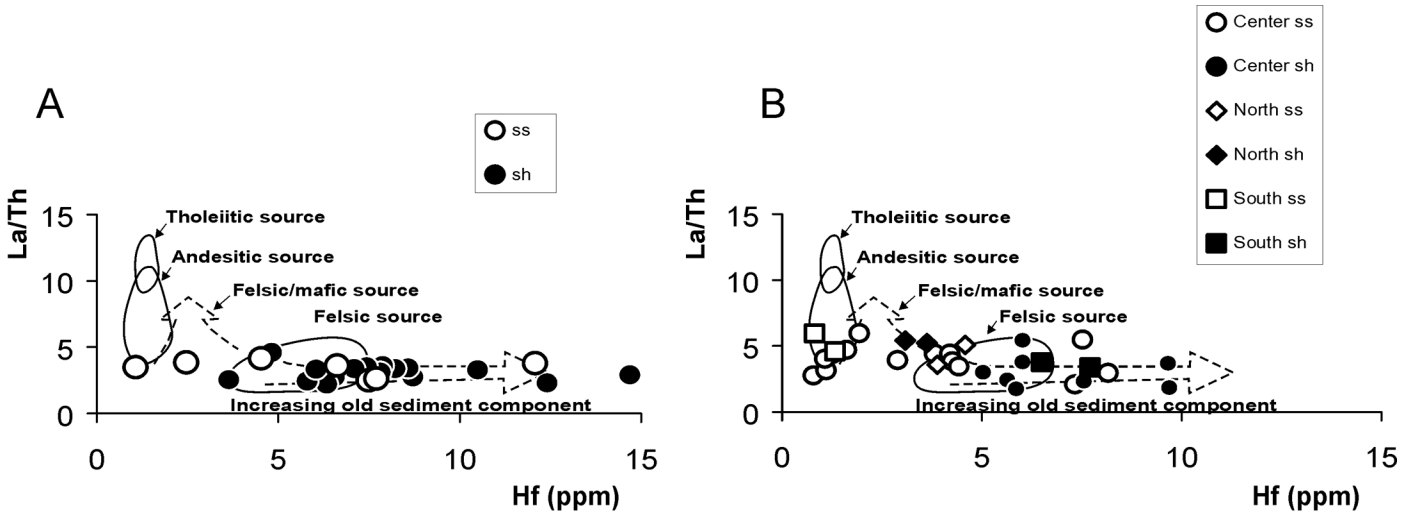

Figure 12. Source rock discrimination diagram (ss—sandstones, sh—shales) (Floyd and Leveridge, 1987) for Permian-Triassic (A) and Lower Cretaceous samples (B).

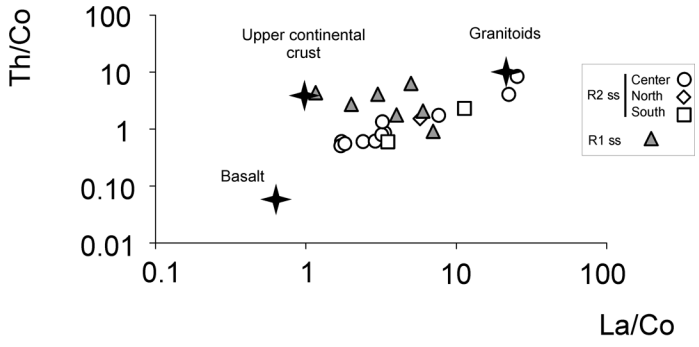

Figure 13. Source-rock discrimination binary diagram (Cullers and Berendsen, 1998), for Permian-Triassic sandstones (rift 1 ss) and Lower Cretaceous sandstones (rift 2 ss). Data about average of granitoids, upper continental crust, and basalts are also plotted.

part of the basin, contemporaneous supplies from a sedimentary cover (Permian-Triassic and Jurassic) were found in association with a volcanic imprint.

CONCLUSIONS

During the most active stages of rifting in the intracratonic Iberian Basin (rift 1: Permian-Triassic; rift 2: Late Jurassic to early Albian), quartzofeldspathic plutoniclastic petrofacies were generated in fluvial-lacustrine environments. Composition of Permian-Triassic sandstones varies in time from very quartzose quartzolithic/quartzofeldspathic at the base of the succession (Saxonian facies) to K-feldspar–rich quartzofeldspathic petrofacies at the top (Buntsandstein facies). This suggests sedimentation in arid conditions and poor maturation during transport. Composition of Berriasian–early Albian sandstones shows variations from proximal areas (quartzofeldspathic petrofacies) to depocentral zones of the basin, as a result of maturation during transport in a humid climate. In addition, sedimentoclastic petrofacies are found in the northern part of the basin. Both Permian-Triassic and Lower Cretaceous deposits are related with a provenance from the Hesperian Massif and its sedimentary cover.

Weathering inferences from geochemical data agree with petrographic deductions. Thus, CIA values in Permian-Triassic sandstones vary between 63 and 73, while in Lower Cretaceous sandstones, these values vary between 71 and 90, reflecting differences in weathering by climate conditions. However, values of CIA can be modified by (1) diagenetic processes in sandstones (illite epimatrix), which increase the Al_2O_3 content; (2) sedimentary supplies from the source area (increasing CaO + MgO content); and (3) allochemical hydrothermalism, which produces an increase in Al_2O_3 by the growth of chlorite minerals.

The use of Th/U ratio could describe a short weathering trend in Permian-Triassic deposits due to the persistent arid conditions during sedimentation. In Lower Cretaceous sandstones, weathering trends are more evident, but with very low ratios and low contents of Th and U.

Geochemical data (major, trace, and REE elements) from both rift 1 and rift 2 deposits fit well in most diagnostic diagrams used for tectonic setting and nature of source rocks.

Ratios between major (Al_2O_3, SiO_2, MgO, K_2O, Na_2O, and Fe_2O_3) and trace elements (La, Th, Sc, Co, and Zr) are in agreement with data from passive-margin settings, in terms of the nature of the crust (Bhatia, 1983; Bhatia and Crook, 1986; Roser and Korsch, 1986). REE values show an enrichment in LREE, a flat HREE pattern, and the characteristic negative Eu anomaly in both rift 1 and rift 2 deposits, suggesting a derivation from an old upper continental crust of felsic nature.

Anomalies such as (1) high content in Sc, Co, and Zr; (2) low content in Hf, Th, and U, and (3) anomalies in ratios like Th/Y, La/Tb, Ta/Y, and Ni/V in some Lower Cretaceous sediments suggest an additional basic source related to alkaline volcanism during Norian-Hettangian and Aalenian-Bajocian times. These volcanic sources could be related to the sedimentary cover (Permian-Triassic and Jurassic) located to the north of the Cameros Basin.

Finally, geochemical composition of rift deposits has manifested to be a useful and complementary tool to petrographic deductions, especially in throwing light on provenance from highly weathered sediments under different climate conditions and maturation during transport. However, many processes affecting the original detrital deposits (e.g., diagenetic processes, hydrothermalism) may produce changes in composition that could bias the provenance and weathering deductions.

ACKNOWLEDGMENTS

The authors thank E. Garzzanti and K. Sircombe for their comments and suggestions in a detailed review of the manuscript. We are grateful to M. Muñoz, M.J. Huertas, C. Villaseca, and J. Escuder for helpful suggestions and their remarks about geochemical data, which consistently improved an early version of the manuscript. Funding for this research was provided by the Spanish Government research projects BTE2001-026 and CGL2005-07445-C03-02.

REFERENCES CITED

Alonso-Millán, A., and Mas, R., 1993, Control tectónico e influencia del eustatismo en la sedimentación del Cretácico inferior de la Cuenca de Los Cameros: Cuadernos de Geología Ibérica, v. 17, p. 285–310.

Alonso-Azcárate, J., Rodas, M., Botrell, S.H., Raiswell, R., Velasco, F., and Mas, J.R., 1999, Pathways and distances of fluid flow during low-grade metamorphism: Evidence from pyrite deposits of the Cameros Basin, Spain: Journal of Metamorphic Geology, v. 17, p. 339–348, doi: 10.1046/j.1525-1314.1999.00202.x.

Arribas, J., 1984, Sedimentología y diagénesis del Buntsandstein y del Muschelkalk de la rama aragonesa de la Cordillera Ibérica (provincias de Soria y Zaragoza) [Ph.D. thesis]: Madrid, Universidad Complutense, 354 p.

Arribas, J., 1985, Base litoestratigráfica de las facies Buntsandstein y Muschelkalk en la rama aragonesa de la Cordillera Ibérica, zona norte: Estudios Geológicos, v. 41, no. 1–2, p. 47–57.

Arribas, J., 1987, Origen y significado de los cementos en las areniscas de las facies Buntsandstein (Rama Aragonesa de la Cordillera Ibérica): Cuadernos de Geología Ibérica, v. 11, p. 535–556.

Arribas, J., Marfil, R., and de la Peña, J.A., 1985, Provenance of Triassic feldspathic sandstones in the Iberian Range (Spain); significance of quartz types: Journal of Sedimentary Petrology, v. 55, no. 6, p. 864–868.

Arribas, J., Alonso-Millán, A., Mas, R., Tortosa, A., Rodas, M., Barrenechea, J.F., Alonso-Azcárate, J., and Artigas, R., 2003, Sandstone petrography of continental depositional sequences of an intraplate rift basin: Western Cameros Basin (north Spain): Journal of Sedimentary Research, v. 73, no. 2, p. 309–327.

Barrenechea, J.F., Rodas, M., and Mas, J.R., 1995, Clay mineral variations associated with diagenesis and low-grade metamorphism of Lower Cretaceous sediments in the Cameros Basin, Spain: Clay Minerals, v. 30, p. 119–133.

Basu, A., Young, S.W., Suttner, L.J., James, W.C., and Mack, G.H., 1975, Re-evaluation of the use of undulatory extinction and polycrystallinity in detrital quartz for provenance interpretation: Journal of Sedimentary Petrology, v. 45, no. 4, p. 873–882.

Benito, M.I., Lohmann, K.C., and Mas, R., 2001, Discrimination of multiple episodes of meteoric diagenesis in a Kimmeridgian reefal complex, north Iberian Range, Spain: Journal of Sedimentary Research, v. 71, no. 3, p. 380–393.

Bhatia, M.R., 1983, Plate tectonics and geochemical compositions of sandstones: The Journal of Geology, v. 91, p. 611–627.

Bhatia, M.R., 1984, Composition and classification of Paleozoic flysch

mudrocks of the Eastern Australia: Implications in the provenance and tectonic setting interpretation: Sedimentary Geology, v. 41, p. 249–268, doi: 10.1016/0037-0738(84)90065-4.

Bhatia, M.R., 1985, Rare earth element geochemistry of Australian Palaeozoic greywackes and mudrocks: Provenance and tectonic control: Sedimentary Geology, v. 45, p. 97–113, doi: 10.1016/0037-0738(85)90025-9.

Bhatia, M.R., and Crook, K.A.W., 1986, Trace elements characteristics of greywackes and tectonic setting discrimination of sedimentary basins: Contributions to Mineralogy and Petrology, v. 92, p. 181–193, doi: 10.1007/BF00375292.

Bhatia, M.R., and Taylor, S.R., 1981, Trace-element geochemistry and sedimentary provinces: A study from the Tasman Geosyncline Australia: Chemical Geology, v. 33, p. 115–125, doi: 10.1016/0009-2541(81)90089-9.

Casquet, C., Galindo, C., González-Casado, J.M., Alonso-Millán, A., Mas, J.R., Rodas, M., García, E., and Barrenechea, J.F., 1992, El metamorfismo en la cuenca de los Cameros: Geocronología e implicaciones tectónicas: Geogaceta, v. 11, p. 22–25.

Cullers, R.L., and Berendsen, P., 1998, The provenance and chemical variation of sandstones associated with the Mid-Continent Rift System, U.S.A.: European Journal of Mineralogy, v. 10, no. 5, p. 987–1002.

Dickinson, W.R., 1985, Provenance relations from detrital modes of sandstones, *in* Zuffa, G.G., ed., Provenance of Arenites: NATO Advanced Science Institutes Series, C-148, p. 333–362.

Dickinson, W.R., and Suczek, C.A., 1979, Plate tectonics and sandstone compositions: American Association of Petroleum Geologists Bulletin, v. 63, p. 2164–2182.

Eynatten, H., Barceló-Vidal, C., and Pawlowsky-Glahn, V., 2003, Composition and discrimination of sandstones; a statistical evaluation of different analytical methods: Journal of Sedimentary Research, v. 73, no. 1, p. 47–57.

Feng, R., and Kerrich, R., 1990, Geochemistry of fine-grained clastic sediments in the Archean Abitibi greenstone belt, Canada: Implications for provenance and tectonic setting: Geochimica et Cosmochimica Acta, v. 54, p. 1061–1081, doi: 10.1016/0016-7037(90)90439-R.

Floyd, P.A., and Leveridge, B.E., 1987, Tectonic environment of the Devonian Gramscatho Basin, South Cornwall; framework mode and geochemical evidence from turbiditic sandstones: Journal of the Geological Society of London, v. 144, no. 4, p. 531–542.

García, D., Ravenne, C., Maréchal, B., and Moutte, J., 2004, Geochemical variability induced by entrainment sorting: Quantified signals for provenance analysis: Sedimentary Geology, v. 171, p. 113–128, doi: 10.1016/j.sedgeo.2004.05.013.

González Menéndez, L., and Suárez, O., 2005, Caracterización petrológica y geoquímica de los diques basálticos de Cadavedo (Valdés, Asturias): Trabajos de Geología, Universidad de Oviedo, v. 24, p. 81–89.

Grigsby, J.D., 2001, Origin and growth mechanism of authigenic chlorite in sandstones of the lower Vicksburg Formation, South Texas: Journal of Sedimentary Research, v. 71, no. 1, p. 27–36.

Gromet, L.P., Dymek, R.F., Haskin, L.A., and Korotev, R.L., 1984, The North American Shale Composite: Its composition, major and trace element characteristics: Geochimica et Cosmochimica Acta, v. 48, p. 2469–2482, doi: 10.1016/0016-7037(84)90298-9.

Gu, X.X., Liu, J.M., Zheng, M.H., Tang, J.X., and Qi, L., 2002, Provenance and tectonic setting of the Proterozoic turbidites in Hunan, south China: Geochemical evidence: Journal of Sedimentary Research, v. 72, p. 393–407.

Guimerà, J., Alonso-Millán, A., and Mas, R., 1995, Inversion of an extensional-ramp basin by a newly formed thrust: The Cameros Basin (N Spain), *in* Buchanan, J.G., and Buchanan, P.G., eds., Basin Inversion: Geological Society [London] Special Publication 88, p. 433–453.

Guimerà, J., Mas, R., and Alonso-Millán, A., 2004, Intraplate deformation in the NW Iberian Chain; Mesozoic extension and Tertiary contractional inversion: Journal of the Geological Society of London, v. 161, no. 2, p. 291–303.

Mantilla-Figueroa, L.C., 1999, El metamorfismo hidrotermal de la Sierra de Cameros (La Rioja, España): Petrología, geoquímica, geocronología y contexto estructural de los procesos de interacción fluido-roca [Doctoral thesis]: Madrid, Universidad Complutense, 361 p.

Martín-Closas, C., and Alonso-Millán, A., 1998, Estratigrafía y bioestratigrafía (Charophyta) del Cretácico inferior en el sector occidental de la Cuenca de Cameros (Cordillera Ibérica): Revista de la Sociedad Geológica de España, v. 11, no. 3–4, p. 253–269.

Martínez-González, R., Vaquer, R., and Lago, M., 1996, El volcanismo Jurásico de la Sierra de Javalambre (Cadena Ibérica, Teruel): Teruel, v. 86, no. 1, p. 43–61.

Mas, R., Benito, M.I., Arribas, J., Serrano, A., Guimerà, J., Alonso-Millán, A., and Alonso-Azcárate, J., 2003, The Cameros Basin: From Late Jurassic–Early Cretaceous Extensión to Tertiary Contractional Inversion—Implications of Hydrocarbon Exploration: Northwest Iberian Chain, North Spain: Barcelona, Geological Field Trip, 11, American Association of Petroleum Geologists International Conference and Exhibition 56 p.

Mata, M.P., 1997, Caracterización y evolución mineralógica de la Cuenca Mesozoica de Cameros (Soria-La Rioja) [Ph.D. thesis]: Universidad de Zaragoza, 349 p.

Mata, M.P., López-Aguayo, F., and Osácar, M.C., 2000, Una aproximación al área fuente del Weald de Cameros: Datos geoquímicas: Geotemas, v. 1, no. 3, p. 263–265.

Maynard, J.B., Valloni, R., and Yu, H.S., 1982, Composition of modern deep sea sands from arc-related basins, *in* Leggett, J.K., ed., Sedimentation and Tectonics on Modern and Ancient Active Plate Margins: Geological Society [London] Special Publication 10, p. 551–561.

McLennan, S.M., and Taylor, S.R., 1991, Sedimentary rocks and crustal evolution: Tectonic setting and secular trends: The Journal of Geology, v. 99, p. 1–21.

McLennan, S.M., Taylor, S.R., and Erriksson, K.A., 1983, Geochemistry of Archean shales from the Pilbara Supergroup, Western Australia: Geochimica et Cosmochimica Acta, v. 47, p. 1211–1222, doi: 10.1016/0016-7037(83)90063-7.

McLennan, S.M., Hemming, S., McDaniel, D.K., and Hanson, G.N., 1993, Geochemical approaches to sedimentation, provenance and tectonics, *in* Johnsson, M.J., and Basu, A., eds., Processes Controlling the composition of clastic sediments: Geological Society of America Special Paper 284, p. 21–40.

McLennan, S.M., Hemming, S.R., Taylor, S.R., and Eriksson, K.A., 1995, Early Proterozoic crustal evolution: Geochemical and Nd-Pb isotopic evidence from metasedimentary rocks, southwestern North America: Geochimica et Cosmochimica Acta, v. 59, p. 1153–1177, doi: 10.1016/0016-7037(95)00032-U.

Nesbitt, H.W., and Young, G.W., 1982, Early Proterozoic climates and plate motions inferred from major element chemistry of lutites: Nature, v. 299, p. 715–717, doi: 10.1038/299715a0.

Nesbitt, H.W., Markovics, G., and Price, R.C., 1980, Chemical processes affecting alkalis and alkaline earths during continental weathering: Geochimica et Cosmochimica Acta, v. 44, p. 1659–1666, doi: 10.1016/0016-7037(80)90218-5.

Ochoa, M., Arribas, J., and Mas, R., 2004, Changes in sandstone composition during Lower Cretaceous syn-rift fluvial sedimentation (Cameros Basin, Spain): Florence, Italy, 32nd International Geological Congress, Abstract CD, Session 242-34.

Pettijohn, F.J., Potter, P.E., and Siever, R., 1973, Sand and Sandstones: New York, Springer-Verlag, 618 p.

Rat, P., 1982, Factores condicionantes en el Cretácico de España: Cuadernos de Geología Ibérica, v. 8, p. 1059–1076.

Roser, B.P., and Korsch, R.J., 1985, Plate tectonics and geochemical composition of sandstones: A discussion: The Journal of Geology, v. 93, p. 81–84.

Roser, B.P., and Korsch, R.J., 1986, Determination of tectonic setting of sandstone-mudstone suites using SiO_2 content and K_2O/Na_2O ratio: The Journal of Geology, v. 94, p. 635–650.

Roser, B.P., and Korsch, R.J., 1988, Provenance signatures of sandstone-mudstone suites determined using discriminant function analysis of major-element data: Chemical Geology, v. 67, p. 119–139, doi: 10.1016/0009-2541(88)90010-1.

Salas, R., and Casas, A., 1993, Mesozoic extensional tectonics, stratigraphy, and crustal evolution during the Alpine cycle of the eastern Iberian basin: Tectonophysics, v. 228, p. 33–55, doi: 10.1016/0040-1951(93)90213-4.

Salas, R., Guimerá, J., Mas, J.R., Martín-Closas, C., Meléndez, A., and Alonso-Millán, A., 2001, Evolution of the Mesozoic Central Iberian Rift System and its Cenozoic inversion (Iberian Chain), *in* Cavazza, W., Robertson, A.H.F.R., and Ziegler, P., eds., Peri-Tethyan Rift/Wrench Basins and Passive Margins: Mémoires du Muséum National d'Histoire Naturelle, v. 186, p. 145–185.

Sopeña, A., and Sánchez-Moya, Y., 1997, Tectonic systems tract and depositional architecture of the western border of the Triassic Iberian Trough (central Spain): Sedimentary Geology, v. 113, p. 245–267, doi: 10.1016/S0037-0738(97)00069-9.

Taylor, S.R., and McLennan, S.M., 1981, The composition and evolution of the continental crust: Rare earth element evidence from sedimentary

rocks: Philosophical Transactions of the Royal Society of London, v. A3, p. 381–399.
Taylor, S.R., and McLennan, S.M., 1985, The Continental Crust: Its Composition and Evolution: Oxford, Blackwell Scientific Publication, 312 p.
Whitmore, G., Crook, K., and Johnson, D., 2004, Grain size control of mineralogy and geochemistry in modern river sediment, New Guinea collision, Papua New Guinea: Sedimentary Geology, v. 171, p. 129–157, doi: 10.1016/j.sedgeo.2004.03.011.
Zuffa, G.G., 1980, Hybrid arenites: Their composition and classification: Journal of Sedimentary Petrology, v. 50, no. 1, p. 21–29.
Zuffa, G.G., 1991, On the use of turbidite arenites in provenance studies: Critical remarks, *in* Morton, A.C., Todd, S.P., and Haughton, P.D.W., eds., Developments in Sedimentary Provenance Studies: Geological Society [London] Special Publication 57, p. 23–29.